Available online at www.sciencedirect.com
ScienceDirect
Organic Geochemistry 38 (2007) 337–364
Organic Geochemistry
www.elsevier.com/locate/orggeochem

Organic matter in the Peruvian headwaters of the Amazon: Compositional evolution from the Andes to the lowland Amazon mainstem

Anthony K. Aufdenkampe [a,*], Emilio Mayorga [b], John I. Hedges [b], Carlos Llerena [c], Paul D. Quay [b], Jack Gudeman [b], Alex V. Krusche [d], Jeffrey E. Richey [b]

[a] *Stroud Water Research Center, 970 Spencer Road, Avondale, PA 19311, USA*
[b] *School of Oceanography, University of Washington, Seattle, Washington, 98195-5351, USA*
[c] *Facultad de Ciencias Forestales, Universidad Nacional Agraria La Molina, Apartado Postal 456, Lima, Peru*
[d] *Centro da Energia Nuclear na Agricultura, Universidade de São Paulo, 13416 Piracicaba, Sao Paulo, Brazil*

Received in revised form 2 March 2006; accepted 1 June 2006
Available online 8 September 2006

Abstract

We examined the compositions of dissolved, fine and coarse particulate organic matter fractions (DOM, FPOM and CPOM, respectively) from 18 river sites in Peru along a 2000 km transect ranging from diverse Andean headwater environments, to depositional reaches, to the confluence of major lowland rivers that form the Rio Amazonas proper. The objective of the study was to evaluate the extent to which compositions of the three primary OM fractions evolve downstream, with the overall goal of assessing the relative effects of various processes in the dynamics of OM within a large river system. Composition was assessed by concentration, elemental (%OC, %N, C/N), isotopic (^{13}C, ^{15}N), hydrolysable amino acid, lignin phenol and mineral surface area analyses. Similar to previous results from the lower Amazon and from Bolivian tributaries, CPOM, FPOM and DOM showed distinct compositional differences from one another. However, compositions of OM size fractions at Andean sites were substantially different from lowland sites, with a clear downstream evolution in most OM properties toward typical lowland Amazon values. Andean FPOM and CPOM both had very high %OC and amino acid content, and low C/N typical of lowland FPOM. Andean UDOM showed low %OC, low C/N, high %TAAC and low non-protein amino acid content – also typical of lowland FPOM. These properties have been shown to be affected by selective partitioning onto minerals [Aufdenkampe, A.K., Hedges, J.I., Richey, J.E., Krusche, A.V., Llerena, C.A., 2001. Sorptive fractionation of dissolved organic nitrogen and amino acids onto fine sediments within the Amazon Basin. Limnology and Oceanography 46 (8), 1921–1935]. In contrast, lignin phenol acid to aldehyde ratios ($(Ad/Al)_v$), indicators of diagenesis, were invariant and within typical lowland values over the entire transect. Thus, we propose that differences in the extent of organo-mineral association are the most plausible explanation for these trends. In the Andes, sand-sized particles appear to be stable aggregates of fine organo-mineral complexes and Andean DOM appears to be complexed with ultra-fine inorganic colloids. Therefore, unlike in previous studies, size was not always a good proxy for the degree of mineral association.

* Corresponding author.
E-mail address: aufdenkampe@stroudcenter.org (A.K. Aufdenkampe).

0146-6380/$ - see front matter
doi:10.1016/j.orggeochem.2006.06.003

However, it appears that selective partitioning of organic carbon and nitrogen molecules may be a dominant process in controlling OM composition in these rivers.

1. Introduction

The Amazon River system is unique for both its geographic extent and the magnitude of hydrologic and biogeochemical fluxes within its channels. Since the physical and biogeochemical processes that take place within the Amazon's waters and watersheds follow the same principles that govern other large tropical river systems, studies of organic matter cycling within the Amazon's diverse and largely pristine rivers have broad applicability to carbon cycle issues at both local and global scales. For these reasons, the Amazon River system has been the focus of an extensive number of important studies on the mechanisms that control the fate and transport of organic matter (OM) in aquatic systems (Hedges et al., 1986b; Amon and Benner, 1996; Keil et al., 1997; Mayer et al., 1998; Richey et al., 2002). These studies, however, have largely focused on the lowland reaches of the Amazon main channel and its largest tributaries. Relatively little is known about the Andean headwaters (McClain et al., 1995), which are the source of over 85% of the sediment load in the mainstem (Gibbs, 1967) and 30–60% of the water discharged to the ocean (Devol et al., 1995).

The CArbon in the AMazon River EXperiment (CAMREX) project has studied the fluxes, transformations and composition of organic matter along a 1800 km reach of the lower Amazon for over 20 years (reviewed by Devol and Hedges, 2001; Mayorga and Aufdenkampe, 2002). One of the more striking findings from these studies is that the three principal size fractions of riverine organic matter – coarse particulate OM (CPOM, >63 μm), fine particulate OM (FPOM, 0.1–63 μm), and dissolved OM (DOM, <0.1 μm) – exhibit distinct compositional characteristics from one another (Ertel et al., 1986; Hedges et al., 1986a; Quay et al., 1992; Hedges et al., 1994; Mayorga et al., 2005a). Furthermore, within each size fraction elemental (C, N), isotopic (^{13}C, ^{14}C) and biochemical (amino acid, carbohydrate, lignin) compositions vary little in space or time along the 1800 km reach of the lower Amazon or between major tributaries (sampled at their mouths). The compositional distinctions between CPOM, FPOM and DOM suggest that these size fractions play functional roles in OM dynamics within the river system.

In brief, these earlier studies showed that CPOM biochemically and microscopically resembles partially degraded tree leaves and other non-woody C3 vascular plant tissues (Hedges et al., 1994). Largely unassociated with minerals and composed of discrete organic particles (Keil et al., 1997), CPOM is equivalent to the low-density (<1.6 g cm^{-3}) fraction of soils. Organic molecules in FPOM are intimately associated with weathered aluminosilicate minerals, with OC/surface-area loadings of 0.5–1.0 mg OC m^{-2} (Keil et al., 1997), as are often observed in soils and sediments (Mayer, 1994a). FPOM is nitrogen-rich and biochemically less degraded than DOM; these patterns appear to result in part from biochemical "fractionation" of DOM as it sorbs to mineral surfaces (Aufdenkampe et al., 2001). Studies in other systems show that organic molecules, once sorbed, are apparently protected and cycle at much slower rates as long as they remain sorbed (Keil et al., 1994; Nelson et al., 1994). DOM is highly degraded and nitrogen-poor (Hedges et al., 1994). In the lowlands, about 60–85% of the DOM is of high molecular weight (HMW > 1000 Da), but decreases in size and bioavailability with degradation to form the low molecular weight (LMW) fraction (Amon and Benner, 1996). Living phytoplankton and bacteria comprise a small fraction of TOC in the river system (Wissmar et al., 1981; Benner et al., 1995).

By showing no downstream evolution of OM these findings could be interpreted as evidence that large river systems act primarily as conduits from land to sea. On the other hand, relatively large microbial respiration fluxes of OM within river waters suggests rather that these large rivers are in dynamic equilibrium with respect to OM sources and losses (Richey et al., 2002). Resolving this question – to what extent do large tropical river systems serve as a pipe vs. as a processor of terrestrial OM – has substantial implications to our understanding of carbon export losses from terrestrial ecosystems and therefore of the global carbon cycle (Schimel et al., 2001; Richey et al., 2002).

One test of the pipe vs. processor hypothesis is to explore whether compositional evolution of riverine

organic matter is apparent farther upstream. In the mid 1990s, the CAMREX project initiated a number of field expeditions to various headwater regions of the Amazon River Basin to employ techniques similar to those used to study the lower reaches of the river system. Hedges et al. (2000) presented the results from the first of those field studies, describing OM compositions along a transect from the Bolivian Andes to the Madeira and eventually to the Amazon mainstem. Here we present results from the second major CAMREX field initiative in the Andes – from a diverse set of Andean environments near the Amazon River source in Peru, down through a range of depositional reaches in the foreland basin, to the confluence of major lowland rivers that form the Rio Amazonas proper (Fig. 1). The objective of this paper is to evaluate the extent to which compositions of the three primary OM fractions evolve downstream, and to consider probable mechanisms for this evolution. The overall goal is to assess the extent to which these rivers simply act as downstream conveyors of OM vs. serving to dynamically process OM inputs that are continuous in space and time.

2. Methods

2.1. Study area

Sampling locations were chosen to follow a detailed transect down one Andean river system (Vilcanota–Urubamba–Ucayali) – from high altitude grasslands, through erosive valleys, through depositional settings, to the Amazonian lowlands (Fig. 1). In addition, because the basin increases from 470 to 341,000 km^2 in area over this transect (sites U1–U13, Table 2), we sampled a number of important tributaries and tributary types. As such a wide diversity of physical environments is presented in this paper (Table 2), this study provides

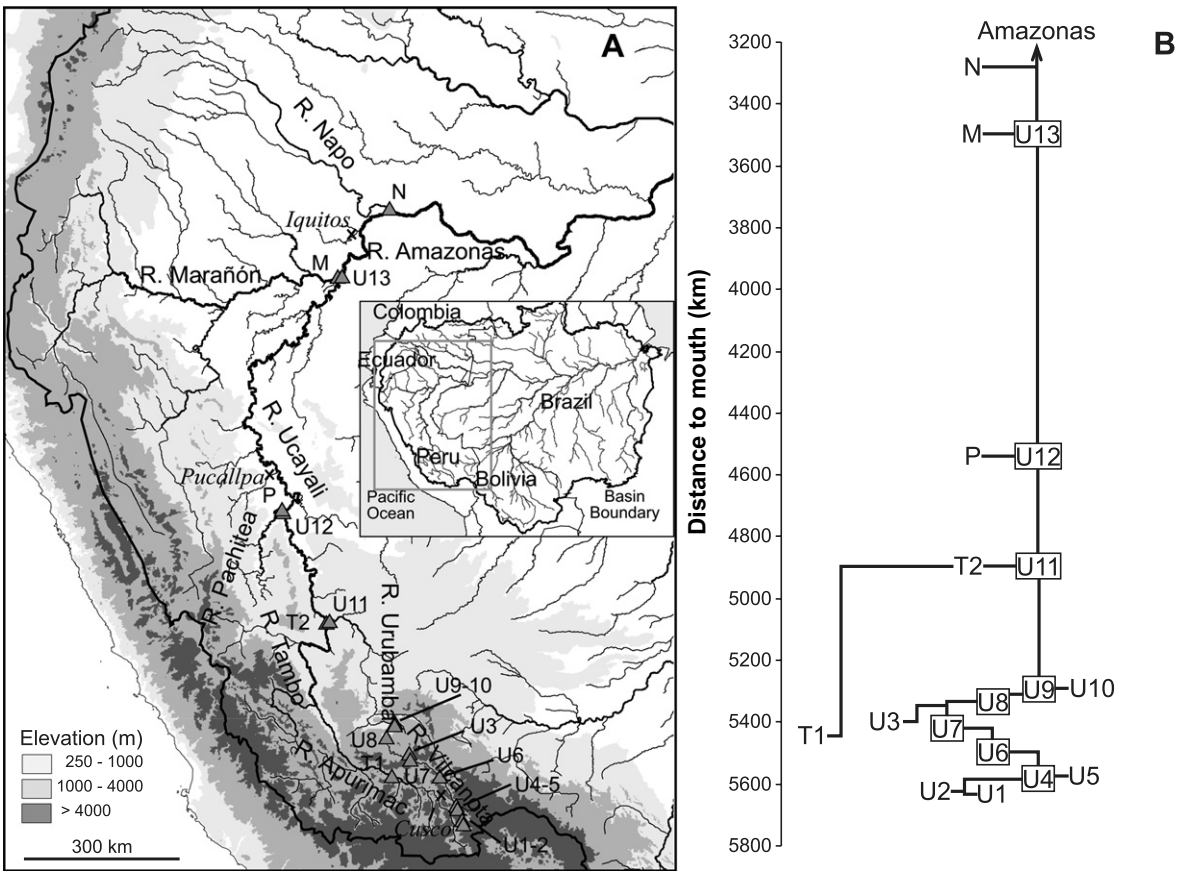

Fig. 1. River sites sampled by the Carbon in the Amazon River Experiment (CAMREX) expedition to Amazon headwaters in Peru, presented (A) in the geographic context of the region and (B) by a schematic of the connections between sites. Vertical distances in B are scaled to actual flow path distances between sites, which are described in Table 1 and in the text.

a relatively complete picture of the waters descending from the Peruvian Andes at the end of the dry season. On the other hand, this diversity of river sites also presents a challenge to simple interpretation of results and often requires placing data from each site into context.

The Amazon River headwaters originate in the Andean Cordillera of southern Peru, just north and west of Lake Titicaca. Here in the high altitude plains (altiplano) and grassland steppes (puna), the Rios Vilcanota and Apurimac begin their long descent to the Atlantic Ocean, a journey of over 6000 km (Table 1, Fig. 1). The Rio Vilcanota begins at Lake Langui-Layo (site U1) at 3970 m elevation and is augmented by affluents from the many wetlands similar to the one sampled (U2), which are scattered across the puna. Shortly after descending into the Vilcanota–Urubamba valley, the Vilcanota (U4) is joined by the larger Rio Salcca (U5), which drains one of the most heavily glaciated massifs in the region. The now muddy Rio Vilcanota continues to flow down the moderately populated valley through several villages and towns, and is joined by streams draining the ancient Inca city of Cusco. One of these streams enters the Rio Vilcanota immediately upstream of site U6. Approximately 210 km after leaving Laguna Langui-Layo, the river, now named the Rio Urubamba, begins to drop (at site U7) down a deeply incised and humid valley by more than 2000 m in less than 100 km to the city of Quillabamba (U8) (Table 1, Fig. 2). The Urubamba flows out of the Andean foothills though cobbled and braided channels (U9) where it is joined by the smaller Rio Yanatili (U10), which was sampled just downstream of the town of Quellouno.

Parallel to the Vilcanota–Urubamba river system flows the larger and longer Rio Apurimac–Rio Tambo river system, which is considered the true headwater of the Amazon River. However, being much less populated and accessible, we were only able to sample the Apurimac in one location (T1) before it descends from the Andes and is renamed the Rio Tambo. The next accessible sampling location was located 550 km downstream in the Andean forelands, at the confluence of the Rio Tambo (T2) with the Rio Urubamba (U11) at the town of Atalaya. At this point the Rio Tambo watershed is nearly twice as large as the Rio Urubamba basin (Table 2). Below their confluence, the river is known as the Rio Ucayali. We next sampled the Ucayali (U12) upstream of its confluence with the Rio Pachitea (P), which increases the watershed area by 12% (Table 2). Below this, near the city of Pucallpa, the river channel is highly sinuous and rapidly migrating (Salo et al., 1986; Puhakka et al., 1992;

Table 1
Sampling locations and characteristics

Site code	River system sampled	Sampling site	Lat. (°S)	Lon. (°W)	Elevation (m)	Distance to mouth (km)	River width (m)	River depth (m)
U1	Lake Langui-Layo	Langui	14.43467	71.28467	3960	5632	–	–
U2	Vilcanota	Altiplano (puna) wetland	14.36317	71.31850	3940	5624	–	–
U3	Santa Maria–Urubamba	Glacier stream	13.15750	72.27483	3800	5397	2-3	0.5
U4	Vilcanota–Urubamba	Tinta	14.14317	71.40300	3490	5582	19	0.9
U5	Salcca	Confluence w/Vilcanota	14.09600	71.43783	3440	5576	29	1.2
U6	Vilcanota–Urubamba	Huanbutio	13.58083	71.71333	3040	5499	24	0.8
U7	Vilcanota–Urubamba	Pachar	13.27417	72.21700	2880	5421	18	2.4
T1	Apurimac–Tambo	Cunyac	13.06300	72.57583	1850	5441	79	5.1
U8	Vilcanota–Urubamba	Quillabamba	12.86600	72.69617	1050	5329	28	nd
U9	Vilcanota–Urubamba	Sahuayaoti	12.64833	72.53500	840	5289	32	5.6
U10	Yanatili	Quellouno	12.63767	72.55717	830	5288	~30	2.1
U11	Urubamba	Atalaya	10.69917	73.74550	290	4889	350	5.2
T2	Tambo	Atalaya	10.74233	73.74483	290	4892	~350	~6
U12	Ucayali	Confluence with Pachitea	8.78417	74.55233	170	4537	700	10.1
P	Pachitea	Confluence with Ucayali	8.75417	74.54300	170	4541	356	7.3
U13	Ucayali–Amazonas	Confluence with Marañón	4.47150	73.43267	110	3498	660	21.3
M	Marañón	Confluence with Ucayali	4.46567	73.49200	110	3500	1400	25.9
N	Napo	Confluence with Ucayali	3.41683	72.69250	100	3280	850	12.2

Latitude and longitude were obtained in the field with handheld GPS units, whereas elevation is a best estimate based on GPS elevations, altimeter readings, site location, and the GTOPO30 digital elevation model (Gesch et al., 1999). Distance to the Amazon mouth into the Atlantic is derived from site locations and Mayorga et al. (2005b) river network dataset. River width and depth were measured in the field.

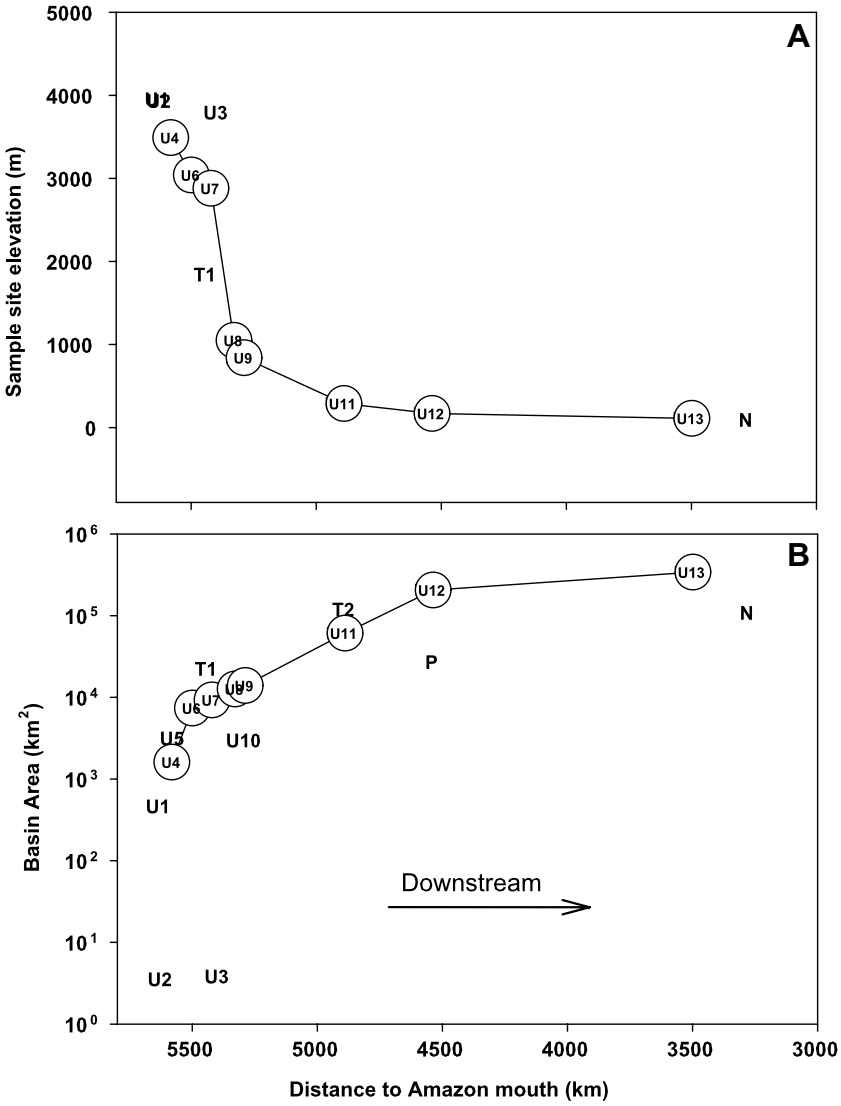

Fig. 2. Downstream trends in (A) elevation of the river surface between sampling sites and (B) upstream watershed area along the confluent Rio Vilcanota–Rio Urubamba–Rio Ucayali flow path (linked symbols) and other sampling sites. See Table 1 for site codes.

Räsänen et al., 1992). Over 1000 km downstream, the equally large Rio Marañón (M) joins the Rio Ucayali (U13) upstream from the city of Iquitos, forming the mainstem river known as Rio Amazonas (Mayorga et al., 2005b). Two hundred kilometers further, the Rio Napo (N) joins the mainstem. Although still 3300 km from the Atlantic, the river is approximately 1 km wide and has fully evolved from Andean streams into a large, lowland tropical river that already has a larger discharge than any other river in the world outside the Amazon (Richey et al., 1986; Ludwig et al., 1996).

The watersheds of the Tambo and Urubamba experience a pronounced seasonality in precipitation as might be expected at 10–15°S latitude due to seasonality in the location of the intertropical convergence zone (Waliser and Somerville, 1994). June to August is typically the driest time of year, receiving only ~25 mm rainfall per month, whereas 150–225 mm per month is typical for January and February. In general, there is a gradient of decreasing precipitation from the eastern slopes of the Andes to the west that is noticeable in the studied watersheds (Table 2). The annual pattern in rainfall is matched by a cycle in temperature. June and July are typically 5 °C colder than October–April. Because of their proximity to the equator, the Rio Marañón and especially the Rio Napo exhibit much

Table 2
Average characteristics of the watersheds upstream of each sampling site

Site code	Area (km^2)	Mean elevation (m)	% Elevation <1000 m	% Elevation >4000 m	Slope (%)	Mean % sand	Mean % clay	Area % forest	Area % woodland	Area % grassland	Mean temperature (°C)	Mean precipitation (mm yr^{-1})
U1	470	4280	0	80.8	8.7	19.5	64.6	0.5	20.8	67.0	7.2	950
U2	<10	4210	0	91.7	4.4	17	67	0	25.0	75.0	8.2	1040
U3	<10	4810	0	100	11.9	83	9	0	38.5	61.5	11.0	990
U4	1610	4240	0	70.5	8.3	21.9	62.4	0.6	22.2	73.8	7.8	1010
U5	3190	4740	0	96.7	5.6	53.6	31.7	0.5	18.7	77.9	8.2	1380
U6	7370	4420	0	75.9	8.3	53.2	33.8	0.5	22.9	73.8	8.7	1220
U7	9290	4280	0	66.0	9.5	59.3	28.7	0.8	27.5	69.4	9.3	1180
T1	22,760	4110	0	61.2	9.4	57.6	31.2	2.7	35.7	61.4	7.8	850
U8	12,640	4000	0.7	56.1	11.7	65.6	23.5	5.6	32.9	59.0	10.1	1120
U9	13,920	3790	3.2	51.0	11.7	67.2	22.1	11.4	32.5	53.9	10.9	1120
U10	3020	3080	1.8	22.4	12.6	82.9	9.0	32.3	43.9	21.7	14.9	1120
U11	61,070	1890	49.3	16.0	7.5	51.9	34.4	63.1	17.6	18.1	18.1	1400
T2	121,290	3200	15.3	37.6	10.4	70.9	19.6	22.9	34.7	41.5	12.3	960
U12	205,520	2500	34.4	27.0	8.6	59.2	29.2	42.7	26.2	29.9	15.4	1200
P	27,500	830	79.1	1.8	4.4	18.1	64.9	86.2	10.7	2.3	22.1	1780
U13	341,200	1660	58.5	16.4	5.8	45.8	38.1	63.0	17.4	18.2	19.3	1520
M	358,170	1110	64.6	2.6	4.8	39.1	44.4	71.1	17.0	10.9	21.6	1720
N	110,300	650	83.6	1.0	2.0	33.0	48.7	86.0	7.2	4.8	23.4	2640

Characteristics extracted from watershed delineations based on Mayorga et al. (2005b) and geographical datasets described in Hedges et al. (2000).

different patterns of seasonality. Low and high water are, respectively, in August and March in the Marañón. The Napo has two annual peaks in rainfall in April–May and October–November. Average basin temperatures are also much more constant in these watersheds.

At the time of sampling in late October and early November 1996, the rainy season had not quite arrived as it typically does in September. Thus, the high elevation rivers (which we sampled first) were sampled at nearly the lowest water stage of the hydrograph. All rivers were sampled just upstream of major confluences. Spatially averaged characteristics of the watershed upstream of each sampling station as calculated from geographic data (more below) are given in Table 2 and are based on datasets and methods described by Hedges et al. (2000). Drainage areas and downstream distances were calculated based on Mayorga et al. (2005b).

2.2. Sampling

At most Andean sites, sampling was performed from bridges. A weighted submersible pump (Shur-Flo DC diaphragm pump) was hung from each bridge into the thalweg (main flow) to 6/10 the total river depth (4/10 from bottom), in order to sample suspended sediment size distributions where water velocities are most representative of depth-integrated fluxes. At lowland sites, the pump was suspended from a drifting boat. Wetland waters were collected by submerging bottles 50 cm, and Lake Langui-Layo was sampled from 2 to 3 m depth at the dam. River depths were monitored with a standard digital fishfinder/sonar (Seaview, Model 600), in which the transducer was mounted on a floating plywood surfboard that could be deployed from bridge or boat. With this method, it was possible to monitor the depth of the pump and the river bottom simultaneously.

At all sites, small and large volume water samples (10 and 60 l, respectively) were collected via the submersible pump for dissolved and fine suspended material. A 63 μm Nitex screen was used to sieve out coarse material. A plankton net constructed from the same 63 μm Nitex screen was used to collect larger amounts of coarse material for chemical analyses. Large volume water samples and coarse suspended sediment (CSS) samples were immediately preserved in the field with $HgCl_2$, to a final concentration of 100 μM. Each evening after sample collection, small volume samples were filtered and processed for various dissolved and particulate analyses for eventual analysis in the laboratory. Care was taken to homogeneously subsample suspended sediments by use of a churn sample splitter (Bel-Art). Dissolved subsamples were preserved with $HgCl_2$ (also to 100 μM) and particulate sam-

ples on filters were immediately dried in a dehydrating oven. Fine suspended sediment (FSS) concentrations were determined gravimetrically, in triplicate, by filtration of a known water volume onto preweighed membrane filters (Millipore HAWP, 0.45 μm pore size). Temperature, pH, and conductivity were analyzed *in situ* using a multi-probe ICM Water Analyzer (''AquaCheck'' Model 51600). At Andean sites, the probe was inserted in an undisturbed sample collected using a horizontal Niskin bottle aligned with the direction of water flow and lowered to 6/10 total river depth at the thalweg; at lowland sites, the probe was lowered directly into the water column.

After being shipped back to the laboratory in the USA, fine particulate and high molecular-weight dissolved materials, or ultrafiltered DOM (UDOM), were isolated from large volume samples with an Amicon DC-10 tangential flow ultrafiltration system using methods described previously (Benner, 1991; Hedges et al., 2000). Briefly, samples were passed through an Amicon H5MP01-43 hollow fiber cartridge (0.1 μm nominal cutoff) to concentrate fine particles to a ~1 l volume. The permeate was then processed a second time, using a S10N1 spiral-wound cartridge (1000 atomic mass unit (amu) nominal cutoff) to concentrate the ultrafiltered dissolved fraction. A freeze drier and a centrifugal evaporator (Jouan RC 10.22) were used to isolate the particulate and dissolved materials, respectively, from these concentrates.

2.3. Chemical analyses

Coarse particulate, fine particulate and ultrafiltered dissolved organic matter were analyzed for total carbon, organic carbon and total nitrogen on a Carlo Erba model 1108 CHN analyzer. Organic carbon was determined after vapor phase acidification (Hedges and Stern, 1984), and inorganic carbon determined by difference between acidified and non-acidified samples. Dissolved organic carbon (DOC) concentrations were measured after acidification and sparging with a modified high temperature combustion MQ Scientific 1001 DOC analyzer (Peterson et al., 2003). CSS, FSS and UDOM isolates were analyzed for %OC, %N, $\delta^{13}C$ and $\delta^{15}N$ by simultaneous elemental analysis-isotope ratio mass spectrometry (EA-IRMS, CE Instruments NC2500 EA coupled to a Thermo-Finnigan DeltaPlus XL IRMS). Stable isotopes are reported using the del notation ($\delta^{13}C$ and $\delta^{15}N$) vs. PDB and atmospheric N_2 standards. Mineral surface areas (SA) of suspended fine and coarse particulates were determined from five-point Brauner–Emmett–Teller isotherms of N_2 adsorption using a Micromeritics Gemini SA analyzer. Prior to SA analysis, organic matter was removed from each sample by multiple treatments with 30% hydrogen peroxide (equilibrated with calcite and quartz) at 50–60 °C for several hours until all bubbling had ceased (Mayer, 1994b). Alkalinity was analyzed on filtered (0.45 μm Millipore HAWP) samples using micro-Gran titration (e.g., Neal, 2001).

Amino acid analysis was performed with reverse-phase high-pressure liquid chromatography (HPLC) of hydrolysates, and quantified vs. charged-matched surrogate recovery standards based on the method of Cowie and Hedges (1992) and described in detail by Aufdenkampe et al. (2001). In brief, samples were spiked with acidic and neutral non-protein amino acids (α-aminoadipic acid (AAAA) and γ-methylleucine (MLeu), respectively) as surrogate recovery standards. δ-Hydroxylysine (HLys), our basic surrogate recovery standard, was not added because of concerns at the time that it might partially degrade during hydrolysis. Samples spiked with charge-matched surrogate standards were then hydrolyzed in 6 N HCl under N_2 in a sealed vial for 70 min at 150 °C. For analysis, amino acids in neutralized hydrolysates were spiked online with *o*-methylthreonine (MThr) as an analytical internal standard, derivatized online with *o*-phthaldialdehyde (OPA), resolved on a 15 cm × 4.6 mm ID C_{18} analytical column (Beckman ODS Ultrasphere, 5 μm pore size) using a binary solvent gradient of methanol vs. aqueous sodium acetate, and detected with a Waters Model 420 fluorometer. Concentrations of each amino acid were corrected for recovery yields of the corresponding internal charge-matched surrogate standards (AAAA for acidic amino acids and MLeu for neutral and basic amino acids).

Lignin phenols were measured using the CuO oxidation method of Hedges and Ertel (1982) as modified by Opsahl and Benner (1995) and Gudeman (unpublished method). Briefly, 30–300 mg of dry solid sample was oxidized by a suspension of CuO in 2 N NaOH under Ar headspace for 3 h within a high-pressure stainless-steel bomb at 155 °C. The reaction solution was then spiked with a nine-compound surrogate recovery standard mixture, acidified, extracted with diethyl ether, dried with Na_2SO_4, evaporated to dryness within a GC autosampler vial, and frozen. Immediately prior to

analysis, reaction products were redissolved in pyridine, spiked with an internal standard and converted to trimethylsilyl (TMS) derivatives by reacting with bis(trimethylsilyl)trifluoroacetamide + 1% trimethylchlorosilane (Regisil) for 30 min at 70 °C. Lignin phenols were separated on a Hewlett-Packard 5890 series II gas chromatograph fitted with a DB-1 fused-silica capillary column (J&W Scientific) and quantified by flame ionization detection (FID). Identities of all quantified peaks were confirmed vs. commercial standards with a Hewlett-Packard 5970 mass selective detector. The average analytical precision was ~10% for the reported lignin phenols.

Missing data in tables and figures generally indicates that insufficient sample quantities precluded making the given measurement.

3. Results

3.1. Concentrations and elemental composition of organic matter size fractions

Concentrations of suspended materials generally increased downstream, but were uncorrelated to basin properties such as average slope. At several sites, stagnant local water conditions – such as in Lake Langui-Layo (U1), or in the wide and deep natural pool/lake at the Apurimac site (T1) – were reflected in low suspended sediment concentrations (Table 3). Even the Vilcanota at Tinta (U4), with steep upstream gradients but above any glacial inputs, only contained 4.5 mg l^{-1} of FSS. On the other hand, waters carried by the glacial stream (U3) and the Rio Salcca (U5) appeared as "glacial milk", having FSS concentrations of 365 and 289 mg l^{-1}, respectively. Through dilution and settling, these concentrations decreased downstream, even below river reaches exhibiting extreme local slopes (between U7 and U8) and through areas of high mean basin slopes (U6–U10). At all lowland reaches (<300 m elevation), fine suspended sediment concentrations were uniformly high, from 179 to 338 mg l^{-1} (Table 3). CSS concentrations at these sites varied more, from 14 to 149 mg l^{-1}. However, these values do not come from flux-weighted sampling methods and CSS is known to show considerable variability with depth and laterally across the channel.

The distribution of organic carbon between coarse particulate, fine particulate and dissolved size fractions varied considerably from site to site (Fig. 3). In general, DOC and FPOC contributed equally to fluxes, with slightly more DOC at many Andean sites and generally more FPOC in the lowlands. CPOC ranged from <1% of total organic carbon (TOC) to 67%, exceeding 450 μM in the puna wetland and the Rio Salcca. High CPOC concentrations in waters at Andean sites were in part a consequence of CSS containing high percents of OC by weight (%OC_{CSS}) (Table 4).

Weight percent organic carbon of both CSS and FSS were much higher at high elevation sites than at any lowlands sites in this or previous studies

Table 3
Sampled water properties, basic chemistry and sediment load

Site code	Sampling date	Temperature (°C)	pH	Conductivity (μS cm^{-1})	Alk (μeq l^{-1})	CSS (mg Sed l^{-1})	FSS (mg Sed l^{-1})	DOC (mg C l^{-1})
U1	24-October-96	11.9	8.46	588	1900		1.5	1.90
U2	24-October-96	18.3	8.40	294	2580	32	10.4	10.65
U3	26-October-96	12.4	7.48	9			365	0.77
U4	23-October-96	18.7	7.69	1160	3320	0.5	4.5	2.63
U5	23-October-96	15.1	7.55	611	2060	60	289	1.32
U6	20-October-96	16.2	8.10	1147	2270	10	81.6	1.94
U7	26-October-96	17.6	7.89	1131	2960	30	184	3.40
T1	21-October-96	22.1	8.75	685	1960	0.5	6.6	1.57
U8	27-October-96	19.7	8.21	428	1390	4.5	55.0	2.41
U9	27-October-96	23.5	8.28	418	1230	4.7	46.7	1.40
U10	27-October-96	23.3	7.67	74	470	18	59.8	1.08
U11	1-November-96	27.0	8.06	146	960	56	268	1.81
T2	1-November-96	25.7	7.91	234	1170	14	251	2.35
U12	5-November-96	26.1	7.70	192	1170	54	289	1.80
P	5-November-96	24.8	7.75	181	1290	55	269	2.21
U13	8-November-96	28.0	7.43	234	1280	31	338	2.65
M	8-November-96	26.0	6.97	134	790	149	333	4.66
N	7-November-96	29.7	6.94	25	270	64	179	2.44

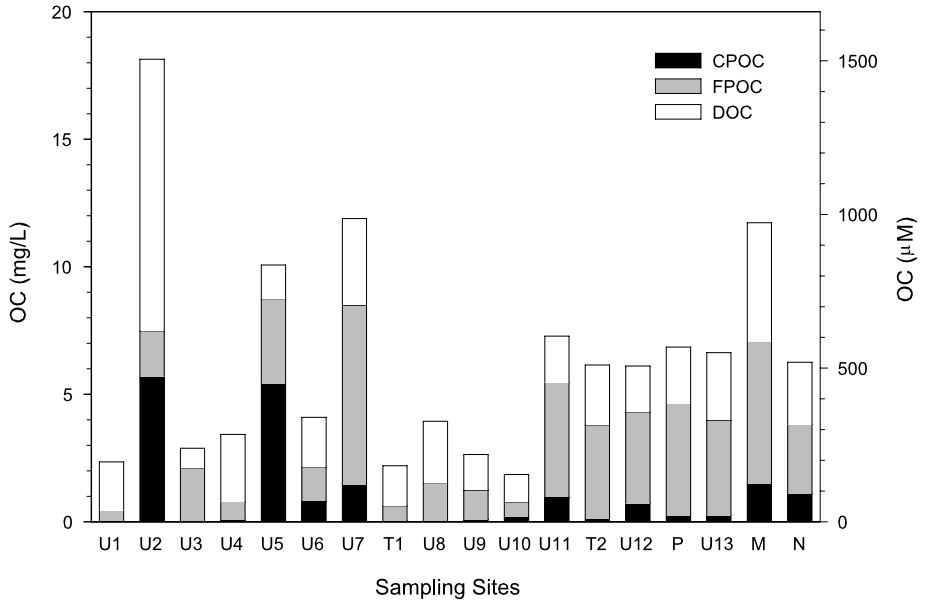

Fig. 3. The concentration of total organic carbon (TOC) in waters sampled at each site, partitioned into contributions from each of the three principle size fractions. Coarse particulate organic carbon (CPOC) is that which is retained on a 63 μm sieve, fine particulate organic carbon (FPOC) passes the sieve but is retained on a 0.1 μm or 0.45 μm filter, and dissolved organic carbon (DOC) passes a 0.1 μm filter.

(Fig. 4A). Measured $\%OC_{CSS}$ values of 18%, 15% and 7.9% at the wetland (U2), Vilcanota at Tinta (U4) and Apurimac (T1), respectively are typical of streams with low suspended mineral content. However, in the Rio Salcca (U5) and lower Rio Vilcanota (U6 and U7) measured values of $\%OC_{CSS}$ of 9.0%, 8.2% and 4.8% are much higher than downstream sites with similar CSS values that have a mean of $1.2 \pm 0.5\%$ (Table 3, Fig. 4A). In contrast, $\%OC_{FSS}$ concentrations increased from 0.6% in a small glacial stream (U3), to 1.2% in the glacial Rio Salcca (U5), to 1.6% and 3.8% farther downstream (U6 and U7). $\%OC_{FSS}$ values subsequently decreased from 2.7% to 2.5% in the foothills (U8 and U9) to uniform values of $1.4 \pm 0.28\%$ at all sites downstream (Fig. 4A). At sites with low FSS (U1, U2, U4 and T1), $\%OC_{FSS}$ was high, ranging from 8.8% to 30%. Thus, patterns in $\%OC_{CSS}$ were not mirrored by patterns in $\%OC_{FSS}$ at all sites. In contrast to particulates, the weight percent of organic carbon in ultrafiltration isolates ($\%OC_{UD}$) showed an increasing trend with decreasing mean basin elevation. At high elevation sites, carbon comprised only 1.0–2.2% of UDOM despite the fact that the ultrafiltration membrane should pass essentially all free dissolved inorganic species (Table 3, Fig. 4A). $\%OC_{UD}$ gradually increased downstream to ~12.5% in the Rio Marañón and Rio Napo (Fig. 4A).

Downstream trends in mineral surface area of particulate fractions closely mirrored trends in weight percent OC (Fig. 4B). Therefore, %OC associated with suspended riverine minerals exhibited much more consistent patterns when normalized to mineral surface area (Table 4, Fig. 5). The surface area of coarse suspended sediments ranged from 3.4 to 7.5 $m^2 g^{-1}$ for lowland sites (Table 4). In contrast, CSS collected at Andean sites exhibited much higher values, ranging from 17.2 to 43.5 $m^2 g^{-1}$. Organic carbon to surface area ratios (OC:SA), excluding the wetland, were 1.9 ± 0.6 mg OC m^{-2} in the lowlands vs. 2.8 ± 0.3 mg OC m^{-2} at Andean sites (Table 4). Similar patterns were observed in the fine fraction. Aside from the 103 $m^2 g^{-1}$ measured for fine material suspended in the wetland, mineral surface area was much more uniform for the FSS fraction, ranging from 11.4 to 45.5 $m^2 g^{-1}$ but showing no distinct downstream trend (Table 4). OC:SA ratios generally ranged from 0.34 to 0.84 mg OC m^{-2}, except for Rio Urubamba sites in the highly depositional foothills (U8 and U9) and the wetland (U2) (Fig. 5).

Molar organic carbon to nitrogen ratios (C:N) for all fractions increased with decreasing mean basin elevation to values typically observed in the lower Amazon mainstem (Fig. 6). In all fractions, samples from the high Andes had lower C:N than

Table 4
Bulk organic matter properties

Site code	Size fraction	Sample symbol	Surface area (m^2/g)	OC (wt%)	IC (wt%)	N (wt%)	Organic C/N (molar)	OC:SA (mg C/m^2)	$\delta^{13}C$ (‰)	$\delta^{15}N$ (‰)
U1	CPOM	C1								
U2	CPOM	C2	43.47	18.0	0.4	2.50	8.4	4.14	−23.8	
U3	CPOM	C3								
U4	CPOM	C4	46.04	14.8	0.3	1.62	10.6	3.21	−26.4	
U5	CPOM	C5	32.14	9.0	0	0.99	10.7	2.81	−25.9	
U6	CPOM	C6		8.2		0.61	15.6			
U7	CPOM	C7	17.17	4.8	3.6	0.62	9.1	2.82	−22.8	
T1	CPOM	CT1	31.80	7.9	1.7	1.05	8.7	2.48	−23.8	
U8	CPOM	C8		0.7	0	0.05	15.6		−26.2	
U9	CPOM	C9		2.0	0	0.12	19.0		−26.0	3.4
U10	CPOM	C10		1.1		0.13	10.2			
U11	CPOM	C11	7.01	1.7	0.1	0.11	18.5	2.47	−28.5	
T2	CPOM	CT2	3.42	0.8	0.5	0.05	17.0	2.22	−28.6	2.1
U12	CPOM	C12	7.49	1.4	0.2	0.09	16.9	1.81	−28.6	
P	CPOM	CP	4.91	0.4	0.4	0.03	16.7	0.85	−29.1	3.0
U13	CPOM	C13		0.8	0	0.06	15.8		−28.2	3.3
M	CPOM	CM	5.63	1.0	0.1	0.06	18.8	1.78	−27.7	2.7
N	CPOM	CN	7.43	1.7	0	0.09	22.7	2.33	−28.6	
U1	FPOM	F1		30.3		3.53	10.0		−26.7	
U2	FPOM	F2	103.9	17.0	1.0	2.63	7.6	1.64	−24.8	
U3	FPOM	F3		0.6		0.12	5.7			
U4	FPOM	F4		16.2	0.6	2.40	7.9		−24.6	
U5	FPOM	F5	24.57	1.2	0.4	0.22	6.2	0.47	−24.7	
U6	FPOM	F6		1.6		0.27	7.0			
U7	FPOM	F7	45.51	3.8	0.7	0.67	6.7	0.84	−23.2	
T1	FPOM	FT1		8.8	1.1	1.24	8.3		−23.7	
U8	FPOM	F8	18.45	2.7	0.4	0.38	8.4	1.48	−24.3	
U9	FPOM	F9	11.40	2.5	0.4	0.34	8.4	2.14	−24.4	
U10	FPOM	F10		1.0		0.16	7.2			
U11	FPOM	F11	25.63	1.7	0.1	0.19	10.4	0.65	−27.1	
T2	FPOM	FT2	27.48	1.5	0.3	0.18	9.5	0.53	−27.6	
U12	FPOM	F12	24.35	1.2	0.2	0.15	9.4	0.51	−28.0	
P	FPOM	FP		1.6		0.20	9.4			
U13	FPOM	F13	32.67	1.1	0.1	0.13	10.1	0.34	−28.6	
M	FPOM	FM	25.46	1.7	0.3	0.16	11.9	0.66	−28.2	
N	FPOM	FN	25.28	1.5	0.2	0.17	10.7	0.60	−28.5	
U1	UDOM	D1		1.4	1.8	0.15	10.6		−23.5	3.8
U2	UDOM	D2		17.0	5.2	1.44	13.8		−25.3	3.9
U3	UDOM	D3								
U4	UDOM	D4		2.2	1.2	0.21	12.1		−23.3	
U5	UDOM	D5		1.0	1.5	0.07	15.7		−21.9	3.2
U6	UDOM	D6								
U7	UDOM	D7		1.6	1.1	0.16	11.6		−22.6	5.7
T1	UDOM	DT1		2.0	1.0	0.16	14.5		−21.8	4.9
U8	UDOM	D8		1.1	2.1	0.08	15.0		−25.2	
U9	UDOM	D9		2.4	1.3	0.16	16.9		−24.8	4.8
U10	UDOM	D10								
U11	UDOM	D11		4.4	3.6	0.23	22.2		−29.0	2.9
T2	UDOM	DT2		5.1	2.8	0.28	21.0		−27.9	3.2
U12	UDOM	D12		4.8	3.5	0.26	21.0		−28.7	3.7
P	UDOM	DP								
U13	UDOM	D13		6.6	3.2	0.31	25.2		−29.5	3.8
M	UDOM	DM		12.5	2.7	0.51	28.8		−29.3	3.6
N	UDOM	DN		12.6	1.7	0.55	26.5		−29.6	4.2

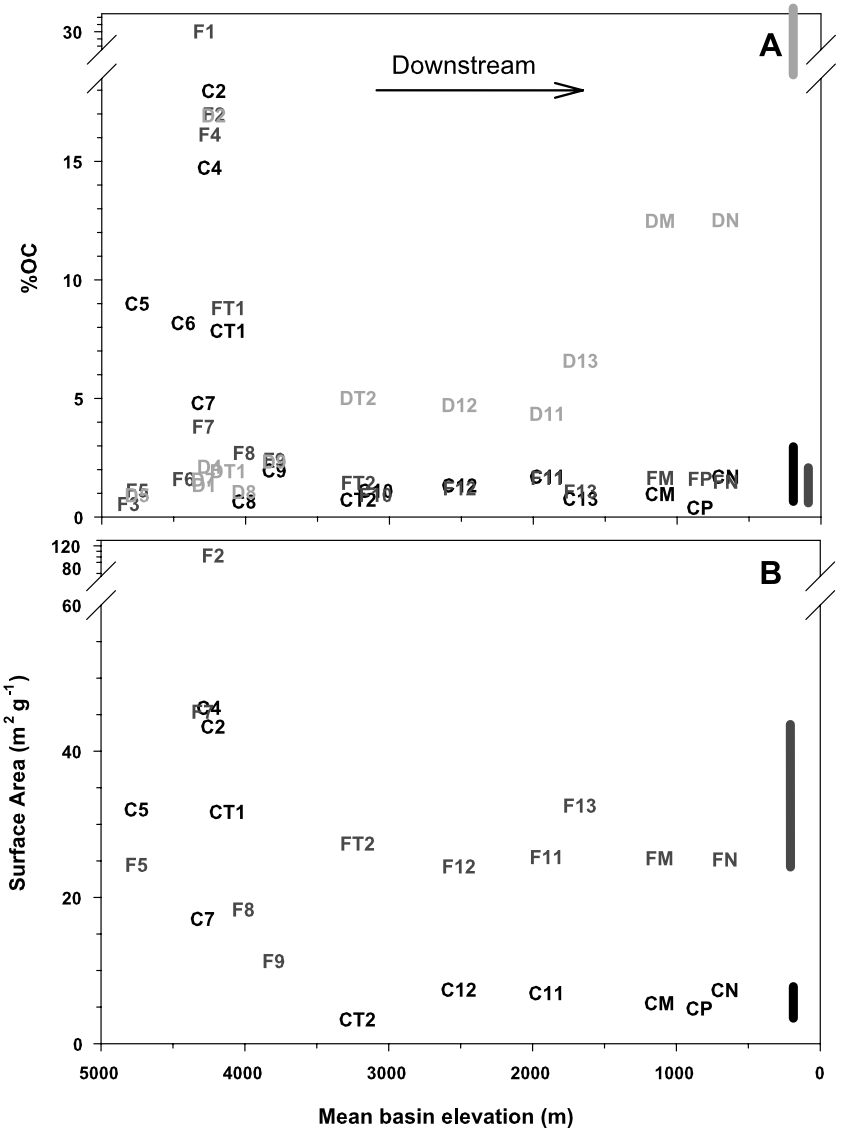

Fig. 4. Downstream trends in (A) percent by weight of organic carbon (%OC) in each of the principal size fractions, and (B) mineral surface area (SA) of particulate fractions, presented as function of mean basin elevation of the watershed upstream from each sampling location. Sample codes are given in Table 4, where the prefixes C, F and D represent coarse particulate, fine particulate and dissolved fractions, respectively. Black, dark grey and light grey bars represent the ranges of typical %OC and mineral SA values (mean ± standard deviation) for CPOM, FPOM and UDOM, respectively, observed in the lower Amazon main channel (Hedges et al., 1986a, 1994; Keil et al., 1997; Mayorga and Aufdenkampe, 2002).

observed previously in the Amazon lowlands (Fig. 6). In general, C:N values were lowest for the FPOM fraction, ranging from 5.7 to 11.9 (Table 4, Fig. 6), whereas CPOM exhibited C:N ratios of 8.4–22.7. Regressions of the data for each particulate fraction (excluding Laguna Langui-Layo) yield relationships $\%OC_{FSS} = (6.55 \pm 0.11) * \%N_{FSS} + (0.16 \pm 0.11)$ and $\%OC_{CSS} = (7.5 \pm 0.4) * \%N_{CSS} + (0.8 \pm 0.3)$ with $r^2 = 0.99$ and 0.96, respectively (Fig. 7). However, the relationship between carbon and nitrogen in CPOM changes at %OC values less than ~2%. Excluding samples with >2% OC_{CSS} and also the Rio Yanatili (U10) changes the regression to $\%OC_{CSS} = (17.6 \pm 1.6) * \%N_{CSS} - (0.14 \pm 0.13)$ with $r^2 = 0.94$ and $n = 9$ (Fig. 7B). Similarly, FPOM along the Urubamba corridor (U5, U6, U8, and U9) shows a strong relationship with a different slope from the main FPOM trend: $\%OC_{FSS} = (10.0 \pm 0.6) * \%N_{FSS} - (1.0 \pm 0.2)$ with $r^2 = 0.99$ (Fig. 7B). What is most striking about this last regression is

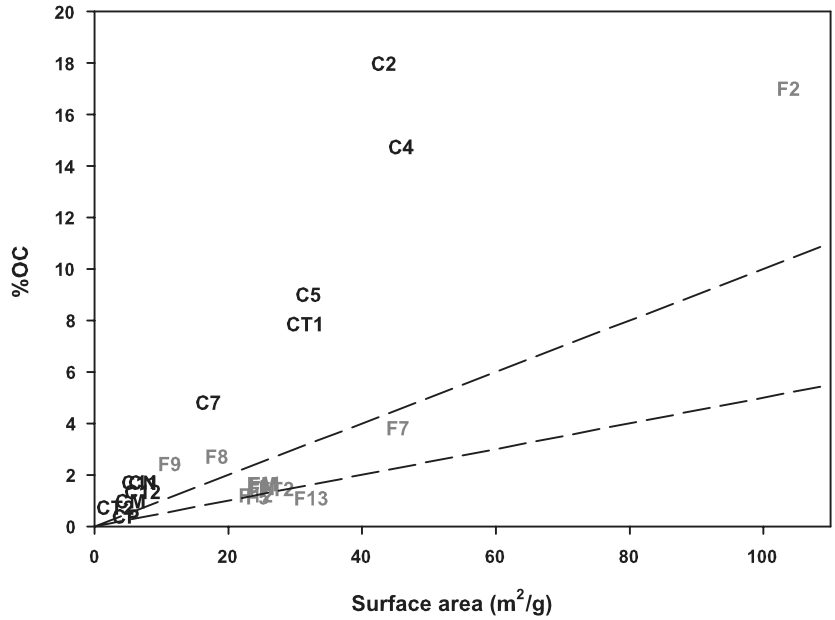

Fig. 5. The weight percent of organic carbon (%OC) as a function of measured mineral surface area (SA) for coarse and fine riverine particulates. Dashed lines bound the region of organic carbon to surface area ratios (OC:SA) of 0.5–1.0 mg OC m^{-2} SA. Sample codes are given in Table 4.

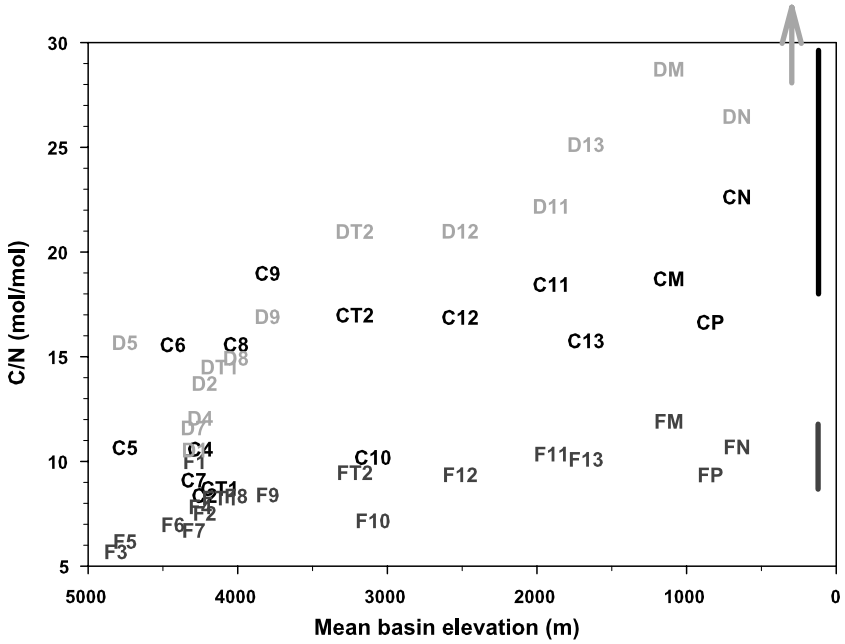

Fig. 6. Downstream trend in carbon to nitrogen ratios. Black, dark grey and light grey bars represent the ranges of values (minimum to maximum) for CPOM, FPOM and UDOM, respectively, observed in the lower Amazon main channel (Hedges et al., 1986a, 1994; Keil et al., 1997; Mayorga and Aufdenkampe, 2002).

an intercept that is statistically different than zero ($p = 0.03$), suggesting that FSS from these locations contain $0.10 \pm 0.01\%$ of inorganic nitrogen. C:N ratios in UDOM appeared to increase steadily downstream (Table 4, Fig. 6), from a mean of 12.8 ± 2.0 at sites greater than 2500 m in elevation

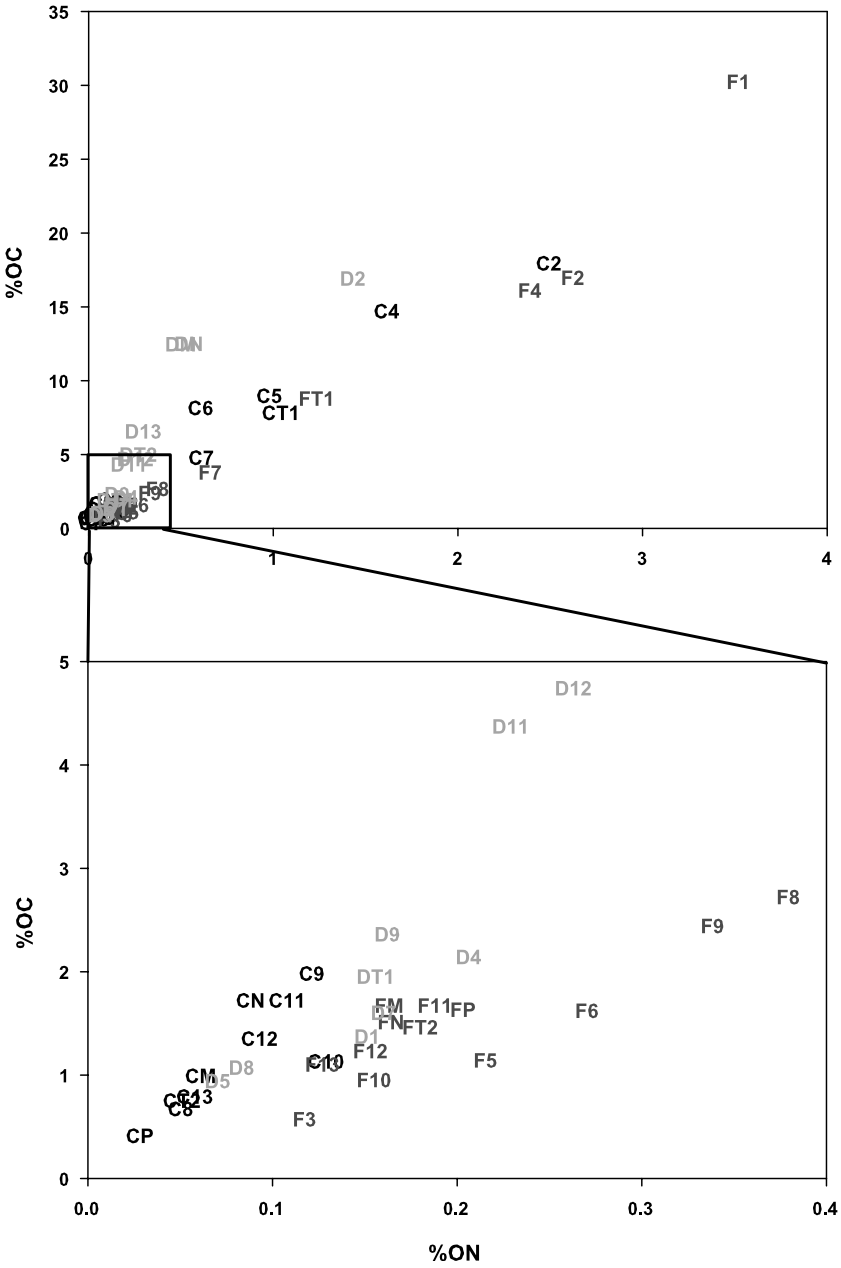

Fig. 7. Weight percent organic carbon as a function of weight percent total nitrogen (%N) for (A) all measured samples and (B) expanded for those samples with lower percent organic concentrations. Sample codes are given in Table 4.

to 27.8 ± 1.8 at the three lowest sites near Iquitos (U13, M and N). Similar to CPOM, the relationship between %OC and %N for UDOM appeared to show a break in slope at ~2% OC, but in the opposite direction (Fig. 7). For all samples with <2.4% OC, the regression is $\%OC_{UD} = (9.5 \pm 2.6) * \%N_{UD} + (0.3 \pm 0.4)$ with $r^2 = 0.72$ and $n = 7$ (Fig. 7B). For all samples with >1.3% OC (excluding the wetland), the regression is $\%OC_{UD} = (29.0 \pm 1.3) * \%N_{UD} - (2.8 \pm 0.4)$ with $r^2 = 0.98$ and $n = 11$ (Fig. 7B). Again, it is worth noting that this intercept is highly different from zero ($p = 0.00005$), suggesting that 0.098 ± 0.01% of the mass of dried UDOM is inorganic nitrogen.

3.2. Stable isotope compositions

Stable carbon isotope signatures ($\delta^{13}C$) of organic matter size fractions were generally greater than −27‰ at Andean sites and less than that downstream (Table 4). These values are best interpreted as a function of mean upstream basin elevation (Fig. 8A). Individual plant species analyzed from the puna, although monocot grasses, showed $\delta^{13}C$ values typical of plants that use the C3 photosynthetic pathway growing at high elevation (Körner and Arnone, 1992; Ménot and Burns, 2001). In general, at any given site, FPOM was enriched in ^{13}C relative to DOM and often relative to CPOM. The exceptions to this trend are generally at low sediment sites (U1, U4 and T1) but also at U7 and the Rio Salcca (U5) where UDOM is enriched by over 3% relative to FPOM (Table 4, Fig. 8A). Stable nitrogen isotope signatures were uniform as a function of elevation or distance down-

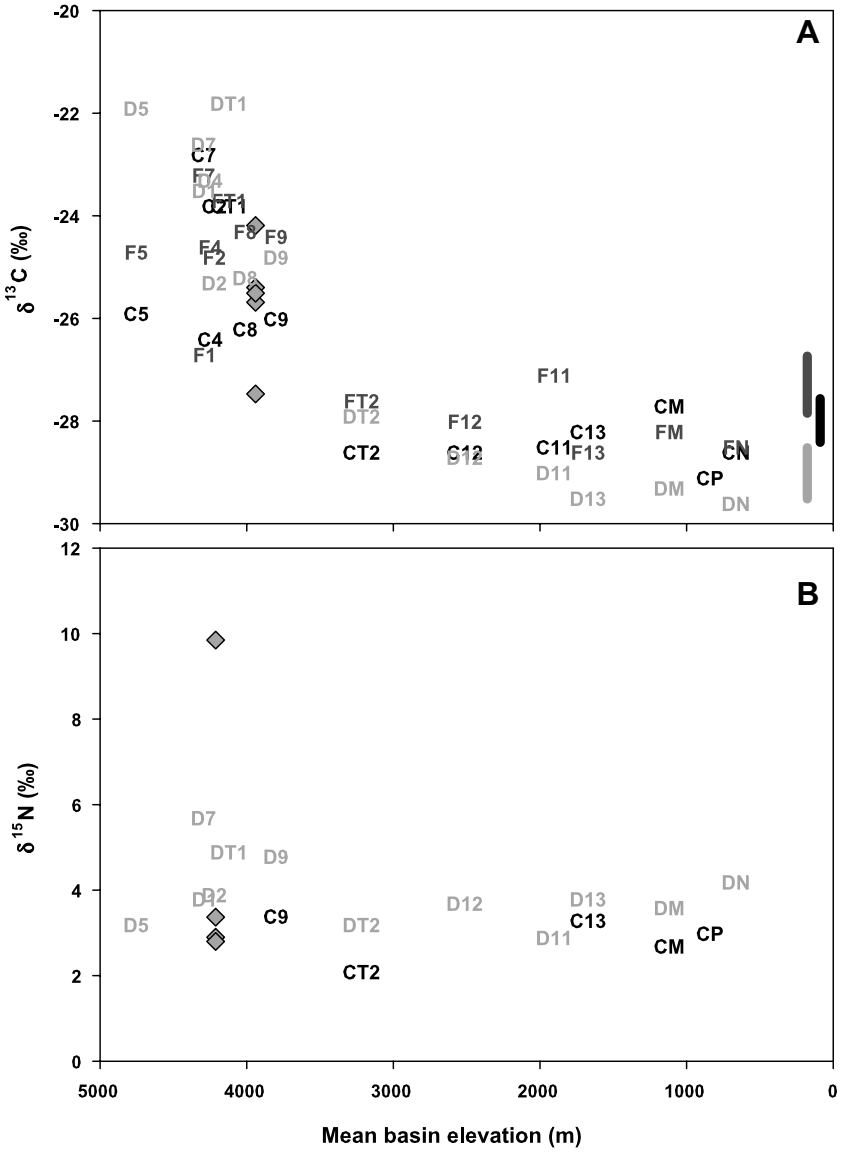

Fig. 8. Downstream trends in stable isotope compositions of (A) carbon ($\delta^{13}C$) and (B) nitrogen ($\delta^{15}N$) for size fractions, as a function of mean basin elevation. Diamonds show values measured for four different plant species (all grasses) collected near site U2. Black, dark grey and light grey bars represent the ranges of typical $\delta^{13}C$ values (mean ± standard deviation) for CPOM, FPOM and UDOM, respectively, observed in the lower Amazon main channel (Quay et al., 1992; Hedges et al., 1994; Mayorga et al., 2005a).

stream. UDOM was generally enriched over CPOM, with average $\delta^{15}N$ values of $4.0 \pm 0.8‰$ and $2.8 \pm 0.3‰$, respectively (Fig. 8B).

3.3. Hydrolyzable amino acids

Total hydrolyzable amino acid yields for 15 protein and three non-protein amino acids clearly decreased from Andean sites to the lowlands for both CPOM and FPOM fractions (Table 5, Fig. 9). From 5% to 28% of the carbon and 10% to 80% of the nitrogen in these samples could be identified chromatographically as these 18 compounds. In general, a larger percentage of nitrogen was identifiable in the CPOM fraction, whereas FPOM contained slightly higher percentages of total amino acid carbon (%T_{AA}C) (Fig. 9). FPOM samples were distinctly divided into two groups, with non-turbid waters (U1, U2, U4 and T1) and waters below Andean population centers (U7, U8 and U9, all likely to have high sewage inputs as evidenced by high ammonium concentrations, not shown) having the highest values of %T_{AA}C and %T_{AA}N. The CPOM fraction from these same sites also had the highest values. The UDOM fraction contained the lowest amino acid yields for all sites and showed no apparent spatial trend.

The distributions of individual amino acids have often been used as proxies for organic matter degradation, especially within marine sedimentary systems (Cowie and Hedges, 1994; Dauwe et al., 1999). Two commonly used parameters are plotted in Fig. 10. The sum of non-protein amino acids β-alanine (βala) and γ-aminobutyric acid (γaba), presented as mole percents of total amino acid yields, has been shown to increase with diagenesis in marine sediments (Cowie and Hedges, 1994). Similarly, an amino acid degradation index (DI), based on factor analysis of 14 protein amino acids from marine sedimentary sequences (Dauwe et al., 1999), is sensitive to subtle of compositional changes that typically accompany degradation. High DI values correlate to relatively fresh sedimentary OM. Analyzed river samples cover the entire range of typical values for each proxy. Most FPOM samples contain less than 1.4% (βala + γaba), with the three lowland samples near Iquitos showing values of 5.0–5.5%. These differences were not directly correlated to DI, although FPOM samples with DI > 1 also had the highest values of %T_{AA}C and %T_{AA}N (Figs. 9 and 10). CPOM values show wide scatter within 0–2.3% (βala + γaba) (excluding the wetland) and 0.0–1.0 DI (Fig. 9). UDOM yielded the most apparent trends. Samples from Andean locations exhibit both low %(βala + γaba) and low DI values, which generally increase to high values of %(βala + γaba) and moderate DI in lowland samples (Fig. 10).

The ratio of basic to basic plus acidic amino acids (B/(B + A)) has been used as a proxy for selective partitioning of organic components onto minerals due to electrostatic interactions (Hedges et al., 1994; Aufdenkampe et al., 2001). B/(B + A) is defined as the ratio of basic amino acids, arginine and lysine, to the sum of these basic amino acids plus acidic amino acids, aspartic and glutamic acid. In general, values for both FPOM and UDOM decreased slightly from the Andean sites to the lowlands, from 0.25 ± 0.03 and 0.09 ± 0.05 to 0.14 ± 0.05 and 0.04 ± 0.04 for FPOM and UDOM, respectively (Fig. 11). These values are considerably lower than those presented previously for three stations along the lower Amazon mainstem (Fig. 11) (Hedges et al., 1994).

3.4. Lignin phenols

Total yields of the eight lignin phenols (Λ) were in general greatest for CPOM samples, ranging from 1.2 to 8.5 mg/(100 mg OC) (Table 6). Yields for FPOM and UDOM samples ranged from 0.3 to 2.4 mg/(100 mg OC). The ratios of lignin phenol groups are commonly used to as proxies for organic matter sources, such as the ratios of syringyl to vanillyl phenols (S/V) and cinnamyl to vanillyl phenols (C/V) (Hedges and Ertel, 1982; Hedges et al., 1986a). Similar to previous observations, lower elevation rivers here showed lignin ratios suggesting leaf material of dicotyledonous plants as the primary source, with possible inputs from woods (Fig. 12). However, the C/V of OM in high elevation rivers exceeded this range and approached values typical of tropical monocotyledonous grasses. In general, CPOM from the upper reaches of the Vilcanota–Urubamba system had the highest values of C/V, followed by FPOM from those same sites. S/V values for these CPOM samples also had slightly higher values than previously observed. The ratio of vanillic acid to vanillin ($(Ad/Al)_v$), which is an indicator of lignin degradation, showed no downstream trends for UDOM and CPOM, with values for each in the range typical of the lower Amazon mainstem (Fig. 13). FPOM showed a similar pattern of nearly constant $(Ad/Al)_v$ values, with the exception of very high values at three upstream sites (U2, U4 and U5).

Table 5
Amino acid composition of the organic matter size fractions

Site code	Size fraction	THAA (mg/100 mg OC)	% TAAC	% TAAN	ASP (mol%)	GLU (mol%)	SER (mol%)	GLY (mol%)	THR (mol%)	ALA (mol%)	TYR (mol%)	MET (mol%)	VAL (mol%)	PHE (mol%)	ILE (mol%)	LEU (mol%)	HIS (mol%)	ARG (mol%)	LYS (mol%)	βALA (mol%)	γABA (mol%)	αABA (mol%)
U1	CPOM																					
U2	CPOM	41.89	18.5	41.6	6.9	7.0	11.1	17.2	7.2	11.8	3.4	1.5	7.1	4.1	4.7	8.5	1.3	3.8	0.7	3.4	0	0.15
U3	CPOM																					
U4	CPOM	37.27	16.4	48.8	7.8	8.1	8.4	21.2	5.6	11.6	2.8	1.2	5.0	4.0	3.9	8.5	1.3	3.3	4.9	2.1	0.15	0.00
U5	CPOM	34.48	15.0	46.9	7.6	6.9	9.2	21.1	6.0	16.4	4.2	0.3	6.0	2.7	3.1	5.9	1.5	2.5	4.0	1.9	0.18	0.32
U6	CPOM																					
U7	CPOM	47.26	20.6	51.3	8.9	8.3	10.5	16.8	7.2	14.5	3.2	0.7	6.3	3.2	3.5	6.2	1.4	3.1	4.0	1.5	0.16	0.28
T1	CPOM	39.86	17.6	43.0	5.2	7.9	9.9	16.6	7.7	15.7	3.1	1.1	7.2	4.1	4.4	6.0	1.5	3.4	3.8	1.9	0.31	0.12
U8	CPOM	26.87	11.8	53.5	10.1	9.0	10.7	15.4	6.4	14.4	3.3	0.0	7.1	3.7	4.0	7.3	1.5	2.8	3.0	0.9	0	0.38
U9	CPOM	29.32	12.9	63.1	9.9	9.0	11.6	14.8	6.5	14.8	3.1	0.2	6.9	3.7	4.1	7.8	1.0	2.6	2.9	0.8	0	0.33
U10	CPOM	60.77	27.1	72.5	6.6	10.7	10.4	13.6	7.1	16.9	3.8	0.4	8.6	4.3	4.6	6.4	1.5	2.5	2.5	0	0	0.21
U11	CPOM	17.15	7.6	36.4	6.0	9.2	11.1	16.6	7.4	14.9	2.6	0.2	7.9	4.0	4.6	5.9	1.9	2.9	3.6	1.3	0	0
T2	CPOM	18.35	8.1	39.1	5.9	9.3	10.3	15.7	7.6	14.7	2.7	0.5	7.8	4.4	4.8	6.5	1.5	3.3	3.8	1.2	0	0
U12	CPOM	15.65	6.9	33.2	6.6	9.7	11.0	16.3	7.4	14.0	2.4	0.3	8.3	4.3	4.6	6.2	1.8	2.7	3.0	1.4	0	0
P	CPOM	18.22	8.1	44.4	5.6	8.6	11.1	15.2	6.7	12.8	2.9	0.5	7.5	3.7	4.4	6.1	2.1	2.8	8.1	1.8	0	0
U13	CPOM	13.60	6.0	29.2	6.6	10.0	10.7	15.7	7.2	13.6	2.6	0.5	7.9	3.8	4.6	6.2	2.3	2.8	4.1	1.5	0	0
M	CPOM	16.43	7.3	38.1	6.8	9.8	10.5	15.5	7.3	14.1	2.5	0.2	7.9	3.9	4.7	6.0	2.1	2.9	3.8	2.2	0	0
N	CPOM	13.59	6.0	40.1	6.7	9.3	11.6	16.0	7.7	14.3	2.2	0.2	7.9	4.0	4.4	5.8	2.1	2.6	3.3	1.8	0	0
U1	FPOM	34.71	15.4	41.5	6.0	13.0	7.8	13.0	7.5	17.0	0.9	0.5	8.1	4.9	5.4	8.3	0.6	4.1	2.2	0.6	0	0.11
U2	FPOM	41.77	18.7	36.4	7.3	14.1	7.4	12.0	7.4	13.9	0.8	1.4	8.5	5.2	6.4	8.1	0.9	3.3	2.0	1.0	0	0.16
U3	FPOM																					
U4	FPOM	39.41	17.4	36.8	6.6	10.4	8.9	13.3	9.4	15.7	0.4	1.1	8.7	4.8	5.7	7.5	0.9	3.5	1.5	1.4	0	0.12
U5	FPOM	13.98	6.1	10.3	6.8	10.2	9.2	14.1	8.7	17.4	0.5	0.5	8.3	4.6	5.3	6.8	0.0	3.3	3.0	0.9	0	0.20
U6	FPOM																					
U7	FPOM	54.71	24.3	45.1	6.2	11.4	7.3	13.4	6.9	16.1	0.8	1.4	8.1	4.7	5.7	7.6	1.1	4.2	3.6	1.4	0	0.07
T1	FPOM	32.15	14.1	31.7	6.5	10.3	8.8	15.0	9.0	15.8	0.4	1.1	8.8	4.7	5.5	7.2	0.6	3.6	1.5	1.1	0	0.12
U8	FPOM	37.93	16.7	38.2	6.5	11.4	8.5	14.2	8.0	15.8	0.4	1.3	8.2	4.8	5.5	7.3	1.0	3.7	2.3	1.3	0	0.14
U9	FPOM	33.84	14.9	33.7	6.7	11.0	8.8	14.9	8.3	16.2	0.3	0.9	8.8	4.8	5.6	7.2	0.5	3.3	1.9	0.7	0	0.12
U10	FPOM																					
U11	FPOM	13.56	5.9	16.6	7.1	10.8	8.4	15.0	8.5	16.2	0.4	0.4	9.1	4.3	5.2	6.6	0.6	2.7	2.0	2.5	0	0.19
T2	FPOM	17.70	7.7	18.5	12.9	11.0	8.1	14.8	8.1	15.6	0.6	0.5	7.9	3.6	4.4	8.6	0.5	1.2	0.9	0.8	0	0.51
U12	FPOM	16.96	7.3	17.9	12.1	10.5	7.6	18.5	7.7	15.1	0.6	0.1	7.2	3.8	4.2	8.0	0.3	1.4	1.4	1.1	0	0.39
P	FPOM																					
U13	FPOM	13.28	5.8	15.6	7.5	11.5	8.3	13.8	7.7	15.3	0.6	0.5	10.1	3.7	4.4	6.1	0.6	2.3	1.7	4.6	0.9	0.23
M	FPOM	12.54	5.5	17.1	7.7	12.1	8.8	14.0	7.7	15.4	0.6	0.6	9.3	3.8	4.6	6.1	0.7	1.7	1.6	4.2	0.9	0.20
N	FPOM	17.13	7.4	20.7	8.2	12.2	8.8	14.2	8.3	15.8	0.5	0.7	8.0	3.9	4.3	6.2	0.5	1.4	1.4	4.4	0.9	0.20
U1	UDOM	4.59	1.7	5.3	6.6	7.7	15.9	14.8	9.2	17.8	3.4	0.0	7.4	4.8	2.8	4.9	0.0	0.7	0.0	0.4	1.2	2.13
U2	UDOM	5.93	2.1	9.2	7.4	8.3	13.9	14.4	9.8	19.8	3.0	0.2	6.2	1.8	2.5	4.2	0.0	1.0	0.3	5.2	1.0	0.90
U3	UDOM																					
U4	UDOM	10.18	3.7	13.7	8.1	7.3	18.3	12.7	14.1	17.3	2.7	0.4	6.7	2.0	2.2	3.8	0.0	1.1	0.7	1.4	0.54	0.80
U5	UDOM	6.55	2.4	11.7	7.4	8.6	19.0	15.5	11.5	15.9	1.7	0.2	6.4	2.5	1.6	3.7	0.0	1.0	2.3	1.2	0	1.42
U6	UDOM																					
U7	UDOM	11.34	4.1	15.2	8.1	8.9	16.8	13.8	11.5	18.6	2.0	0.0	6.2	2.0	2.3	3.7	0.0	1.6	1.4	1.6	0.57	0.99
T1	UDOM	8.19	3.0	13.1	8.6	9.0	17.6	11.0	14.3	18.9	1.8	0.4	7.5	2.0	2.3	3.9	0.0	0.8	0.5	0.7	0	0.66
U8	UDOM	6.64	2.4	11.0	8.1	9.7	13.2	17.6	9.5	16.7	1.4	0.0	7.9	2.9	2.9	4.9	0.0	0.5	0.0	1.8	1.9	1.25
U9	UDOM	7.64	2.8	14.4	9.4	9.2	13.6	16.4	11.0	16.8	1.6	0.1	7.5	2.3	2.9	4.8	0.0	0.8	0.7	1.4	0.9	0.64
U10	UDOM																					
U11	UDOM	6.12	2.2	14.8	10.5	9.5	11.3	16.3	7.9	13.0	1.0	0.6	10.6	3.5	3.6	6.5	0.0	0.7	0.6	2.1	1.5	0.83
T2	UDOM	5.06	1.8	11.9	9.6	10.0	11.4	16.9	7.8	13.7	1.4	0.4	8.0	3.6	3.5	6.4	0.0	1.2	1.4	1.7	1.7	1.16
U12	UDOM	4.20	1.5	9.5	10.0	8.4	8.6	17.4	9.2	15.6	1.7	0.3	7.9	3.8	3.4	5.6	0.0	0.0	0.0	4.0	2.5	1.67
P	UDOM																					
U13	UDOM	4.05	1.5	11.2	10.8	8.5	8.9	19.7	8.0	15.1	1.4	0.2	8.1	3.2	3.5	6.0	0.0	0.3	0.0	3.9	1.8	0.74
M	UDOM	3.00	1.1	9.4	12.0	7.3	9.8	17.5	9.6	15.3	1.3	0.2	8.6	3.0	3.3	5.6	0.0	0.3	0.0	2.9	2.4	0.94
N	UDOM	3.48	1.3	10.0	11.0	8.6	7.8	17.1	8.0	15.3	1.3	0.3	9.2	3.2	4.0	6.6	0.0	0.0	0.6	4.3	1.8	0.85

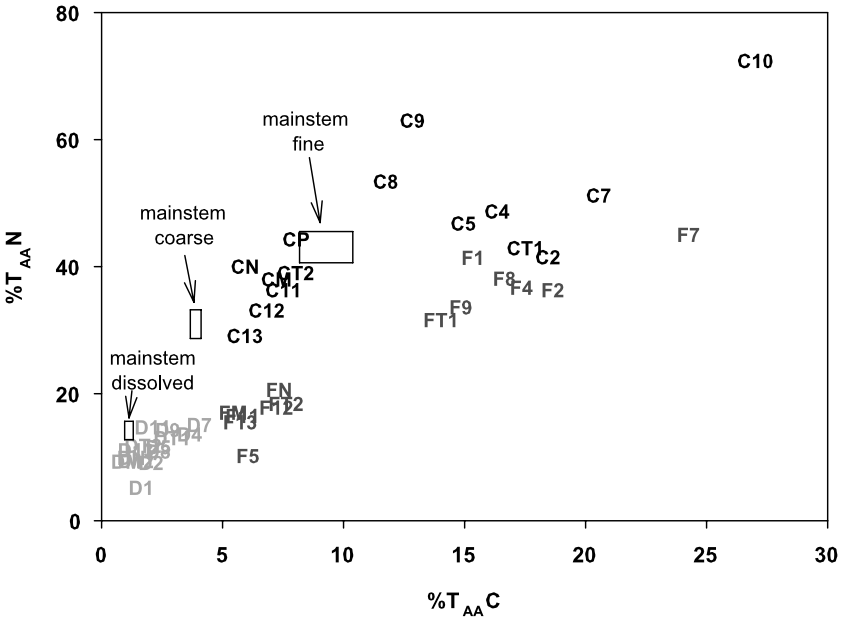

Fig. 9. The percent of total organic nitrogen identifiable as amino acids ($\%T_{AA}N$) as a function of the corresponding percent total amino acid carbon ($\%T_{AA}C$). Boxes encompass the ranges of values observed in the lower Amazon main channel (Hedges et al., 1994).

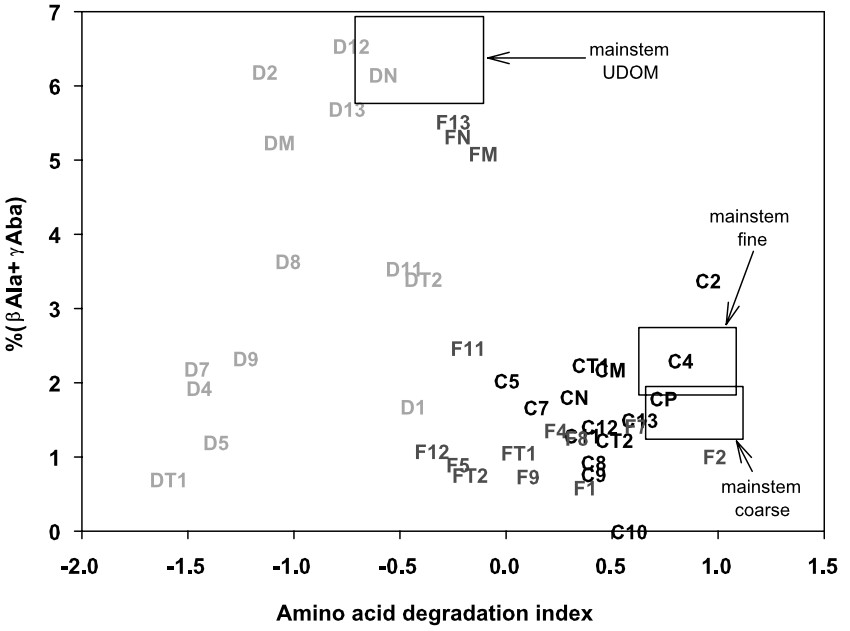

Fig. 10. The percent contribution (to total amino acids) of non-protein amino acids β-alanine and γ-aminobutyric acid (%(βala + γaba)), as a function of an amino acid degradation index developed by Dauwe et al. (1999). Boxes outline the mean ± standard deviation values for mainstem Amazon River samples measured by Hedges et al. (1994).

4. Discussion

The following discussion is directed toward answering the overall question of whether processes within the river system play an active role in transforming organic matter during transport or whether organic matter compositions merely reflect a mixing of materials from various sources.

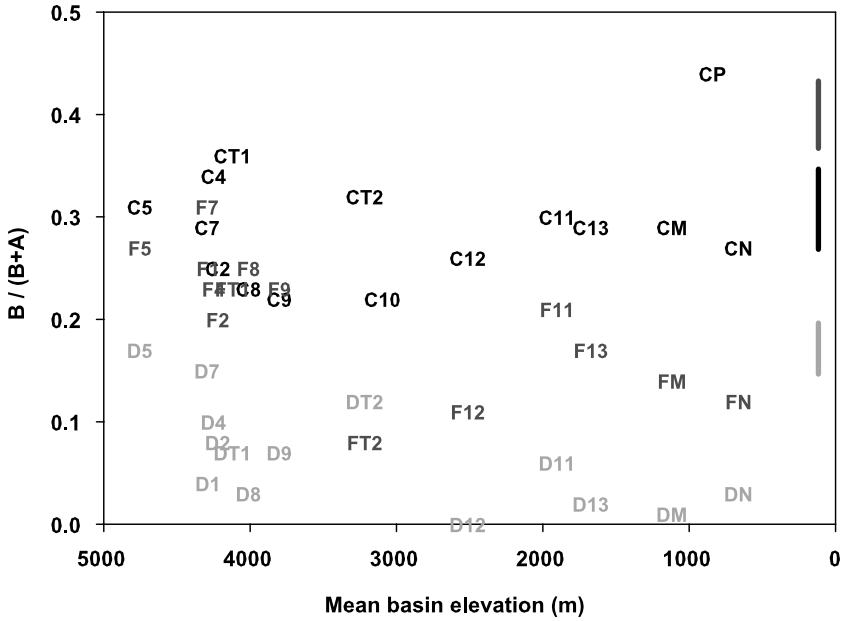

Fig. 11. Downstream trends in the ratio of basic amino acids, arginine and lysine, to the sum of these basic amino acids plus acidic amino acids, aspartic and glutamic acid (B/(B + A)), presented as a function of mean basin elevation. Black, dark grey and light grey bars represent the ranges of (B/(B + A)) values (minimum to maximum) for CPOM, FPOM and UDOM, respectively, observed in the lower Amazon main channel by Hedges et al. (1994).

Therefore, particular attention is given to evaluating the likely mix of processes (source vs. degradation vs. partitioning) that determine OM compositions at given locations and whether this mix is consistent with observed downstream trends.

Previous discussions of organic matter compositions in river systems (Hedges et al., 1994, 2000; Devol and Hedges, 2001) have divided isotopic and biochemical evidence into classes of parameters that discern the sources of OM vs. those that indicate its relative extent of degradation. Most recently, we have demonstrated that the process of selective partitioning between dissolved and particulate phases is a third process that must be considered when interpreting isotopic and biochemical compositional signatures. Two recent studies by our group demonstrated experimentally that mixing natural DOM with aluminosilicate minerals results in newly mineral-associated OC that is enriched in nitrogen (N/C), total hydrolyzable amino acids (%TAAC and %TAAC), basic amino acids (B/(B + A)) and stable carbon isotopes ($\delta^{13}C$), and depleted in non-protein amino acids (βala, γaba and αaba) (Aufdenkampe et al., 2001). As such, we were able to recreate in a beaker the major nitrogen compositional patterns of organic matter transported by the Amazon. Of particular importance is that this selective partitioning between dissolved and mineral-associated OM fractions appeared to be entirely responsible for differences in several compositional signatures that have previously been interpreted as indicators of differing source or diagenesis (Aufdenkampe et al., 2001). This is not to say that these indicators, which were mostly developed to interpret sedimentary sequences in marine settings, are no longer useful. They certainly have a wide basis of evidence supporting comparisons between mineral-associated organic matter at different sites (Cowie and Hedges, 1994; Cowie et al., 1995; Wakeham et al., 1997). Rather, the new findings on sorptive compositional fractionation highlight the difficulty in comparing indicators of source or diagenesis between dissolved, mineral-associated and mineral-free particulate fractions. Therefore, we will first address evidence for sorptive partitioning of organic matter between particulate and dissolved fractions, then discuss apparent sources to these fractions and finally evidence for diagenesis within fractions, all with an eye for trends of downstream compositional evolution.

Organic matter distributions. The finding that coarse and fine sediments were generally most concentrated in waters at lowland sites (downstream of

Table 6
Lignin phenol yields, in mg/(100 mg OC), of the organic matter size fractions

Site code	Size fraction	Lambda Λ	VAL	VON	VAD	SAL	SON	SAD	CAD	FAD
U1	CPOM									
U2	CPOM	1.21	0.33	0.13	0.21	0.17	0.12	0.08	0.07	0.10
U3	CPOM									
U4	CPOM	2.05	0.42	0.13	0.16	0.48	0.29	0.16	0.21	0.20
U5	CPOM	3.37	0.85	0.23	0.26	0.77	0.26	0.24	0.40	0.36
U6	CPOM									
U7	CPOM	3.19	0.61	0.28	0.36	0.45	0.32	0.39	0.39	0.38
T1	CPOM	3.31	0.92	0.24	0.28	0.91	0.28	0.24	0.22	0.23
U8	CPOM									
U9	CPOM									
U10	CPOM									
U11	CPOM	8.46	2.98	0.71	0.65	2.30	0.65	0.49	0.38	0.30
T2	CPOM									
U12	CPOM									
P	CPOM									
U13	CPOM									
M	CPOM									
N	CPOM									
U1	FPOM									
U2	FPOM	1.10	0.16	0.08	0.33	0.20	0.11	0.07	0.03	0.11
U3	FPOM									
U4	FPOM	0.67	0.10	0.03	0.16	0.11	0.06	0.06	0.05	0.10
U5	FPOM	0.45	0.08	0.03	0.08	0.09	0.07	0.04	0.03	0.04
U6	FPOM									
U7	FPOM	0.83	0.17	0.07	0.09	0.15	0.11	0.08	0.06	0.10
T1	FPOM	0.96	0.23	0.07	0.14	0.23	0.12	0.07	0.04	0.06
U8	FPOM	1.50	0.30	0.08	0.20	0.38	0.18	0.13	0.07	0.15
U9	FPOM	1.74	0.43	0.13	0.23	0.44	0.15	0.14	0.08	0.16
U10	FPOM									
U11	FPOM	1.90	0.51	0.14	0.30	0.49	0.16	0.17	0.06	0.08
T2	FPOM	2.30	0.65	0.20	0.35	0.53	0.20	0.20	0.07	0.10
U12	FPOM	2.11	0.56	0.17	0.30	0.57	0.20	0.16	0.06	0.09
P	FPOM									
U13	FPOM	1.98	0.51	0.15	0.33	0.54	0.17	0.16	0.03	0.10
M	FPOM	2.23	0.62	0.19	0.34	0.59	0.18	0.18	0.05	0.08
N	FPOM	2.40	0.68	0.20	0.34	0.66	0.19	0.18	0.05	0.09
U1	UDOM									
U2	UDOM	1.00	0.23	0.12	0.24	0.14	0.12	0.07	0.02	0.07
U3	UDOM									
U4	UDOM	0.32	0.06	0.05	0.07	0.02	0.08	0.02	0.01	0.03
U5	UDOM									
U6	UDOM									
U7	UDOM	0.31	0.06	0.05	0.07	0.02	0.06	0.03	0.00	0.03
T1	UDOM	0.36	0.08	0.05	0.11	0.03	0.05	0.02	0.01	0.01
U8	UDOM	0.70	0.15	0.09	0.20	0.08	0.07	0.07	0.01	0.03
U9	UDOM	0.79	0.18	0.10	0.17	0.13	0.08	0.07	0.02	0.05
U10	UDOM									
U11	UDOM	2.24	0.49	0.24	0.48	0.43	0.21	0.24	0.05	0.10
T2	UDOM	1.80	0.41	0.22	0.44	0.29	0.16	0.18	0.02	0.08
U12	UDOM	1.16	0.27	0.16	0.31	0.17	0.11	0.11	0.01	0.02
P	UDOM									
U13	UDOM	1.37	0.27	0.16	0.36	0.24	0.13	0.13	0.02	0.07
M	UDOM	1.81	0.40	0.21	0.43	0.33	0.16	0.19	0.02	0.07
N	UDOM	1.78	0.39	0.20	0.42	0.35	0.15	0.17	0.02	0.09

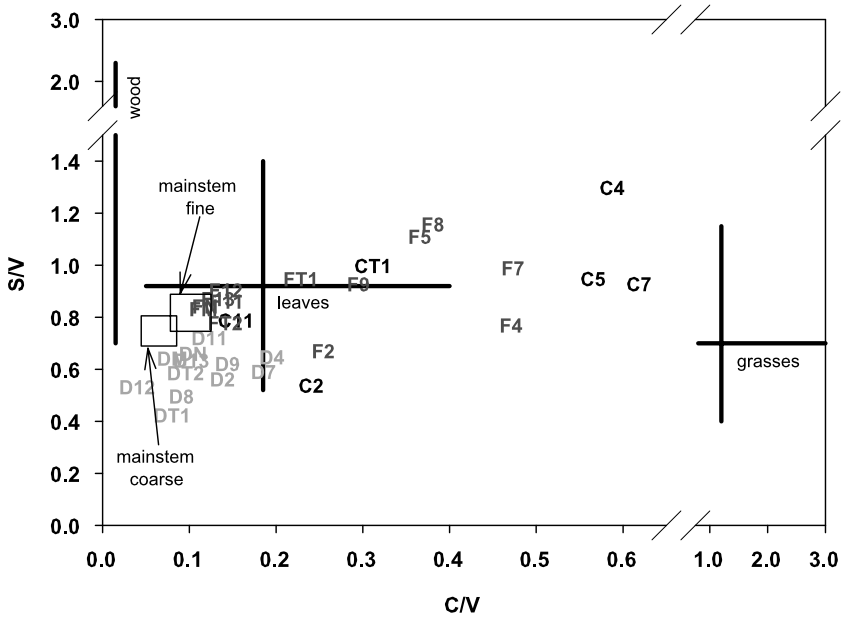

Fig. 12. Lignin compositional parameters, the weight ratios of syringyl to vanillyl phenols (S/V) and cinnamyl to vanillyl phenols (C/V). Crosses represent the median and range of values measured for monocotyledonous grasses, dicotyledonous plant leaves and woody tissues by Hedges et al. (1986a). Boxes outline the mean ± standard deviation values for mainstem Amazon River samples measured in the same study.

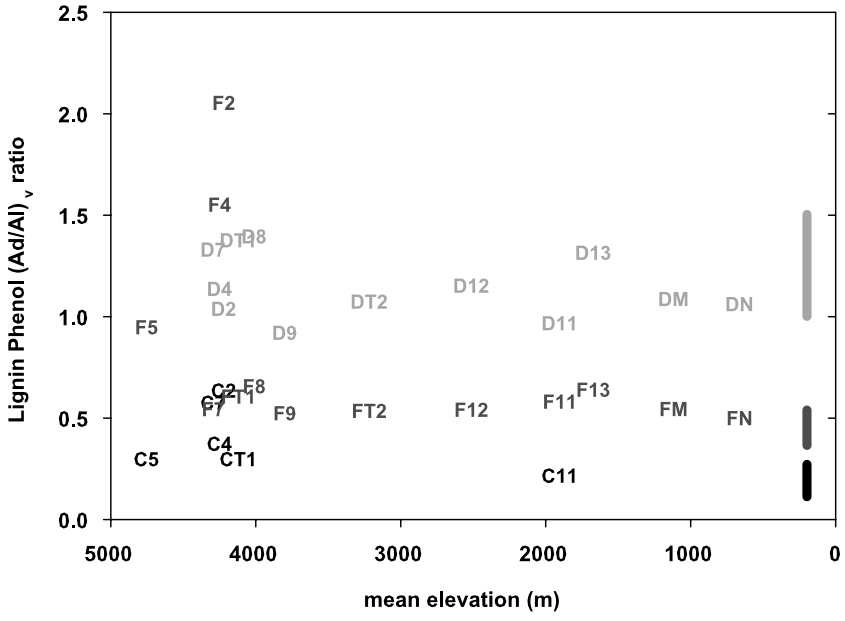

Fig. 13. Downstream trends in the weight ratio of acidic to aldehyde lignin vanillyl phenols $(Ad/Al)_v$, presented as a function of mean basin elevation. Black, dark grey and light grey bars represent the ranges of $(Ad/Al)_v$ values (minimum to maximum) for CPOM, FPOM and UDOM, respectively, observed in the lower Amazon main channel (Ertel et al., 1986; Hedges et al., 1986a).

U10) – which exhibit both the lowest local slopes and mean basin slopes – is not immediately intuitive (Table 3), nor has such a trend been documented previously to our knowledge. However, the Andean rivers were sampled late in the dry season. Typically, small erosive mountain rivers mobilize most of their annual sedimentary load during the severest storms of the year (Aalto et al., 2003), leaving their beds

scoured and armored with large grained material for the remainder of the year. On the other hand, rivers in net depositional environments are generally characterized by rapid channel migration in which more sediment is exchanged between banks than is transported downriver (Dunne et al., 1998; Aalto et al., 2003). The seasonal range of sediment concentrations observed in the upper reaches of the Brazilian Amazon (i.e. at Vargem Grande, Devol and Hedges, 2001) bracket CSS and FSS values from lowland sites in our study. Thus, observations during our sampling expedition in October–November 1996 are not inconsistent with observations elsewhere.

Particulate organic matter concentrations (Fig. 3) not only reflected these patterns in suspended sediments, but also the OM content associated with those sediments. Although most $\%OC_{CSS}$ and $\%OC_{FSS}$ values observed in our study were typical of those measured in turbid rivers throughout the Amazon lowlands (0.6–3.3% and 0.5–2.0%, respectively) (Mayorga and Aufdenkampe, 2002), several sites in the Andes provided notable exceptions (Fig. 4). High %OC values, especially for CPOM, appear to be explainable in large part by variations in mineral surface area (Fig. 5). Although expected for FPOM, the strong relationship between %OC and SA came as a surprise for the coarse fraction. Data from the lower reaches of the Amazon show that most organic matter in the larger size fractions is found as discrete particles that have no physical associations with mineral material (Keil et al., 1997). The surface areas of these coarse fractions are also generally low, $<8\ m^2\ g^{-1}$ (Keil et al., 1997; Aufdenkampe, unpublished data). CSS collected in all lowland sites in this study (below 500 m elevation) show similarly low surface areas (Table 4). In contrast, measured surface areas for CSS at high altitude sites were large (17–46 $m^2\ g^{-1}$), higher than any other riverine CSS samples anywhere in the Amazon Basin including Bolivia (Aufdenkampe, unpublished data).

These surface area data suggest that the >63 μm particle fraction at upland sites might be composed of robust aggregates of much finer material that are likely in close physical association with organic matter. This hypothesis was confirmed by environmental scanning electron microscopy (ESEM) of CSS and FSS at lowland and upland sites (Fig. 14). At moderate magnification (101×), CSS from all sites clearly appears as a mixture of particles in the range of 50 to 200+ μm in diameter (Fig. 14A and C), whereas FSS requires higher magnification to resolve individual particles, which appear to range from 1 to 30 μm in diameter (Fig. 14E and F). However, when the CSS is viewed at higher magnification (1001×), coarse particles from high altitude sites clearly appear to be aggregates of much finer minerals (Fig. 14B), whereas CSS particles at lowland sites visibly contain at their core large mineral grains >50 μm (Fig. 14D). These visual patterns from ESEM are consistent with surface area data – all CSS samples with surface area exceeding $17\ m^2\ g^{-1}$ appear in ESEM images as aggregates of fine minerals whereas all remaining CSS samples (ranging from 3 to $8\ m^2\ g^{-1}$) are clearly dominated by large minerals.

Elemental composition. Relationships between the carbon and nitrogen contents of river samples offer an informative look at OM dynamics. At lowland sites on the Amazon mainstem and major tributaries, previously published C/N of CPOM ranged from 18 to 30 (Hedges et al., 1986a, 1994, 2000), which is typical of the low density (<1.6), mineral-free organic fraction of soils (Oades, 1989; Amelung et al., 1998) and only slightly lower than the leaves of most tropical plants (Hedges et al., 1986a). CPOM from sites with elevation <1500 m in our study generally fell in this range of C/N values (Table 4) and followed a slope of 17.6 ± 1.6, corresponding to a molar C/N of 20.5 ± 1.9 (Fig. 7), which is nearly identical to C/N of CPOM from the Amazon mainstem and major tributaries (Hedges et al., 1994). In contrast, at sites >1500 m elevation CPOM exhibited C/N ratios that were substantially lower, and a regression of this data yielded a slope of 6.5 ± 1.0 corresponding to a molar C/N of 7.5 ± 1.2 (Fig. 7). These values are indistinguishable from the slope for all FPOM samples presented here and also for FPOM samples from the Amazon mainstem and major tributaries (Hedges et al., 1994). These observations, coupled with %OC and SA data, further support the hypothesis that CSS exported from puna and high altitude environments is composed of aggregations of finer minerals. Furthermore, two observations suggest that physical processes may disaggregate the CPOM into FPOM before it reaches the lowlands. The distinct characteristics of high elevation CPOM disappear immediately after descending the short, steep and very turbulent reach between sites U7 and U8 (~1000 m drop in ~15 km, or a 7% grade, near Machu Picchu, http://earth.google.com/). At the same time, FPOM samples from U8 and U9 have OC/SA ratios that are strikingly similar to those observed for the upstream CPOM samples.

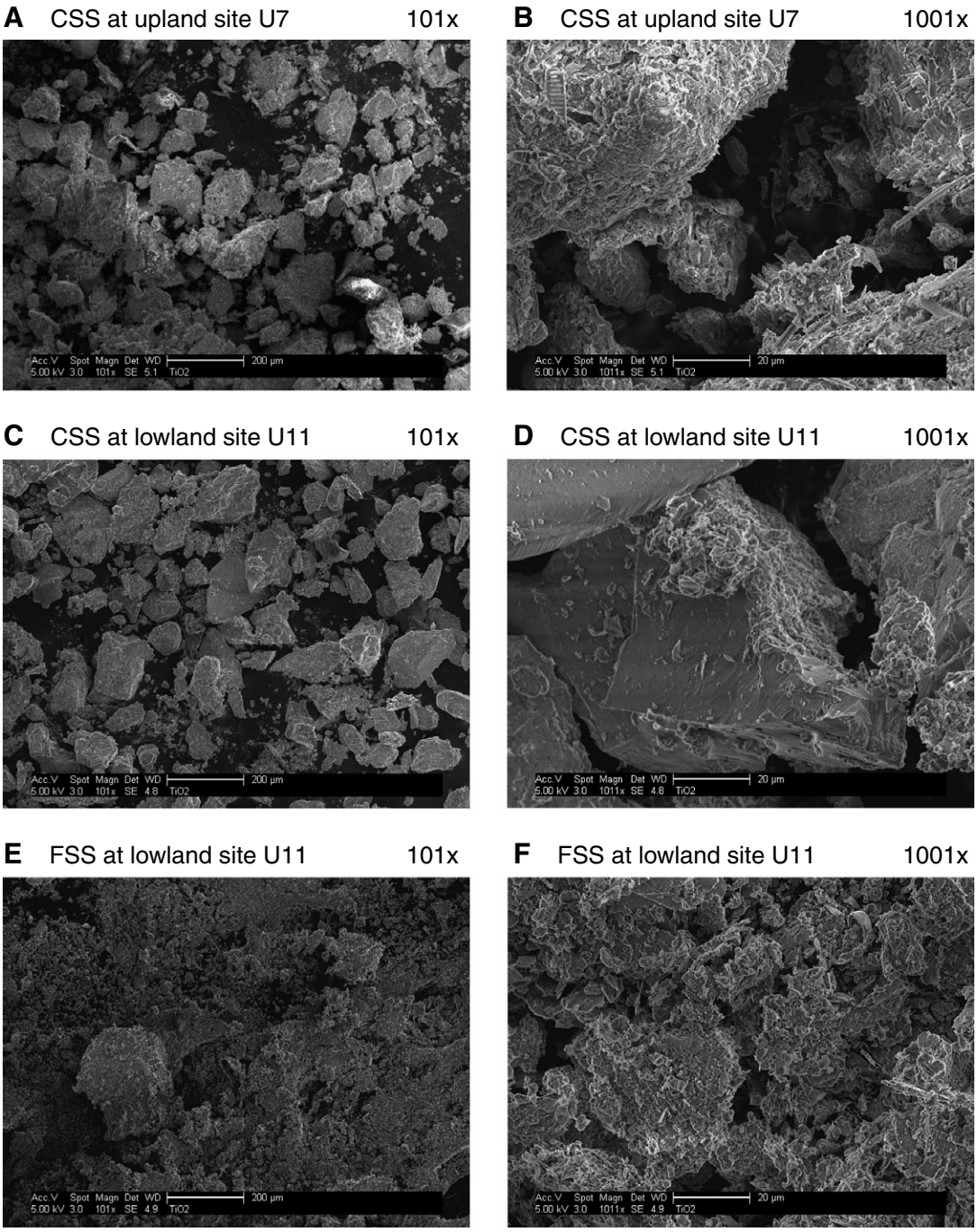

Fig. 14. A comparison of environmental scanning electron microscope (ESEM) images of riverine coarse and fine suspended sediments (CSS and FSS) from two contrasting sites. Images on the right (B, D, F) are a 10× zoom of the images on the left (A, C and E). Scale bars shown within each image are 200 and 20 μm on the left and right sides, respectively.

FPOM samples exhibited relationships between %OC, %N and SA that are all very similar to previous observations of FPOM throughout the basin (Hedges et al., 1994; Keil et al., 1997). However, at many of the same locations, CPOM with similar surface areas and C/N ratios exhibited OC:SA ratios that were 2–4 times higher than is typically found in FPOM or downstream CPOM. These high

values may be due to additional protection offered by these aggregates, which are known to protect OM in soils (Oades, 1989; Baldock and Skjemstad, 2000).

Ultrafiltered dissolved organic matter isolates at high elevation sites had remarkably low %OC of 1–2%, which increased downstream to values at the Rios Napo and Marañón (~12%) that were still less than half of what has been observed further downstream in the Amazon mainstem (24–36%) (Hedges et al., 1994). This pattern was very similar to that observed for the Rio Beni system of Bolivia (Hedges et al., 2000). These $\%OC_{UD}$ values also appear to be a function of river water conductivity (Fig. 15), where $\%OC_{UD}$ generally decreases with increasing conductivity to 400 $\mu S\,cm^{-1}$, above which $\%OC_{UD}$ remain between 1% and 3%. Although such high inorganic contents in ultrafiltration isolates might at first glance appear to be due to high salt content, simple inorganic cations and anions should easily pass through a 1000 Da ultrafiltration membrane. However, inorganic complexes may indeed be retained by the membrane. Another explanation is that inorganic colloids, formed by the physical breakdown of chemically unweathered substrates, may be mobilized into cold Andean rivers prior to extensive chemical weathering or dissolution. The explanation that low %OC is due to inorganic complexes and colloids rather than simple salts is supported by the strong correlation between $\%OC_{UD}$ and C/N, excluding the puna wetland with no mineral inputs ($r^2 = 0.80$, $p = 0.00004$). Such colloids would likely dissolve once transported to warmer regions, although dilution with non-Andean waters could equally explain downstream trends.

Isotopic composition. Stable carbon isotopic signatures have a long history of use as a tracer of carbon sources. In addition to its usefulness in distinguishing between tropical grasses and other plants (C3 vs. C4 photosynthetic pathways) and in identifying marine and freshwater planktonic sources, $\delta^{13}C$ is valuable as a tracer of high elevation inputs. C3 plants typically exhibit increases of 0.7–1‰ in $\delta^{13}C$ values for every 1000 m gain in elevation (Korner and Arnone, 1992; Bird et al., 1994; Ménot and Burns, 2001). Samples from high altitude sites in our study reflect these enrichments, and others have observed similarly high $\delta^{13}C$ values in riverine particulates of −24‰ to −25‰ at other locations within the high Andes (Cai et al., 1988; Hedges et al., 2000; Townsend-Small et al., 2005). Based on such values and signatures of −27.4‰ for FPOM in the Amazon at Obidos, Hedges et al. (2000) estimate that >60% of FPOM originates in the lowlands despite the fact that >85% of FSS originates from the Andes.

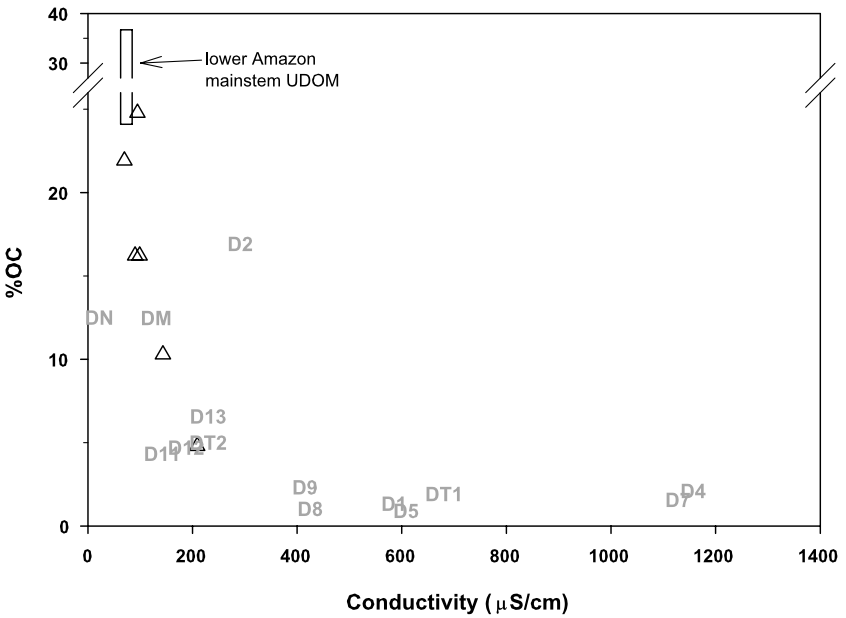

Fig. 15. Weight percent organic carbon of ultrafiltered dissolved material ($\%OC_{UD}$) as a function of river water conductivity. Triangles show data from the Rio Beni river system in the Bolivian Andean Amazon (Hedges et al., 2000), and the box encompasses the ranges of values observed in the lower Amazon main channel (Hedges et al., 1994).

The question here is whether the enriched Andean signal is the cause for the consistent 1–2‰ offset between FPOM and UDOM (Fig. 8). One argument is that if FPOM exchanges with local OM pools more slowly than UDOM, then this delay could cause FPOM to become more enriched than UDOM as they are transported downstream. However recent experimental results demonstrate that sorption and related processes can be responsible for a 1–3‰ enrichment in newly mineral-associated OM relative to the parent DOM (Aufdenkampe, unpublished data). One test of whether these fractionations are important in the Amazon River system is to see if the characteristic 1–2‰ offsets also occur at the highest elevation sites. In our study, only three out of the seven sites with mean basin elevations >3000 m show FPOM to be enriched over UDOM (Fig. 8). On the other hand, $\delta^{13}C$ signatures of UDOM are extremely variable between these samples with the highest values greatly exceeding measured values for plants in this region. It may be possible that the high inorganic carbon (IC) contents of these samples (roughly equivalent amounts of OC and IC; Table 4) may make isotopic measurement difficult. With a $\delta^{13}C$ signature of ~0‰, incomplete acidification and volatilization of even small amounts of inorganic carbon could strongly affect results. Another test of whether sorptive fractionation ^{13}C might be responsible for offsets between FPOM and UDOM is to see whether downstream decreases in the $\delta^{13}C$ of FPOM lag decreases in the $\delta^{13}C$ of UDOM. Clearly, our data do not show such a lag. The $\delta^{13}C$ of FPOM reaches a quasi-plateau almost immediately below 4000 m mean basin elevation, and $\delta^{13}C$ values for FPOM and UDOM roughly run parallel to each other below this. In short, although the data from this study confirm values for the high elevation end members of each size fraction, there is not enough data to robustly determine whether offsets between fractions result from this altitudinal gradient or from fractionations during organo-mineral association.

Biochemical composition. Andean and lowland sites distinguished themselves based on amino acid compositions of both coarse and fine particulates (Fig. 9). $\%T_{AA}C$ values for Andean CPOM was substantially higher than previously measured CPOM from the lower Amazon mainstem (3.7–4.1%) and major tributaries (5.2–5.7) (Hedges et al., 1994) and from Bolivian rivers (3.3–7.7%) (Hedges et al., 2000). On the other hand, FPOM from these same sites in the Peruvian Andes showed only slightly higher values than those from the Amazon mainstem (8.2–10.4%) and similar values to major lowland tributaries (7.2–17.0%) (Hedges et al., 1994). Because recent findings show that amino acids exhibit strong preferential partitioning to minerals (Aufdenkampe et al., 2001), these results lend strong support to our earlier hypothesis that the CPOM fraction at these locations is composed of tightly associated organo-mineral aggregates. $\%T_{AA}N$ has also been shown to reflect selective partitioning (Aufdenkampe et al., 2001), although less so than $\%T_{AA}C$. However, $\%T_{AA}N$ is also sensitive to diagenesis (Cowie and Hedges, 1994). Because we observed minimal differences in CPOM composition between Andean vs. lowland sites despite large differences in the degree of mineral association, it is possible that differences in $\%T_{AA}N$ between size fractions, particularly at the lowland sites, predominantly reflect differences in the extent of degradation between fractions. Similar patterns in lignin phenol acid to aldehyde ratios further support this hypothesis (more below).

Two other amino acid parameters – %(βala + γaba) and DI – have also been shown to respond to both diagenesis (Cowie and Hedges, 1994; Dauwe et al., 1999) and selective partitioning (Aufdenkampe et al., 2001). The cross-plot thus shows the complex interaction of the two processes on determining amino acid distributions in riverine OM. CPOM all plotted in a cluster at relatively high DI values and relatively low %(βala + γaba), suggesting relatively fresh organic matter. DI values for FPOM are spread from 1.0 to −0.5, generally decreasing downstream with apparently increased biodegradation. The values of %(βala + γaba) are uniformly low for most FPOM samples. This could signal that these sediments have freshly partitioned OM associations that have not yet had time to develop the high %(βala + γaba) values that appear at the three sites furthest downstream (F13, FM and FN) that are located below extremely active zone of sediment deposition and erosion and channel migration (Salo et al., 1986; Räsänen et al., 1992). UDOM samples demonstrate best that these biochemical degradation proxies may be sensitive to other processes. Andean samples exhibit both very low DI and %(βala + γaba), with values generally increasing downstream. This pattern reflects in many ways a mirror image of the trend with FPOM samples. That is, sites that show highest DI values for FPOM show the lowest DI values for UDOM. Sites where DI values are the lowest for FPOM

show the highest values for UDOM. This inverse pattern strongly suggests that partitioning reactions may determine DI values for the two fractions. These observations of natural riverine OM thus lend support to previous experimental findings (Aufdenkampe et al., 2001) that amino acid signatures can not be easily used to interpret diagenetic differences between mineral-associated organic matter and either DOM or mineral-free POM.

The one compositional parameter that has previously been used to infer selective partitioning is B/(B + A) (Hedges et al., 1994). In the Amazon mainstem, this parameter clearly shows that basic amino acids are enriched in FPOM and depleted in UDOM relative to CPOM, which is considered to most closely resemble the biochemical source of OM in these rivers (Fig. 11). For the entire Peruvian sample set, both values for B/(B + A) for FPOM and UDOM are depleted relative to CPOM, as was observed in Bolivia (Hedges et al., 2000). Lower B/(B + A) values in the more recent datasets can be partially explained by differences in the application of charge-matched surrogate recovery standards. In the datasets in this paper, in Hedges et al. (2000) and in Aufdenkampe et al. (2001), no basic surrogate recovery internal standard was added (see Section 2) and basic amino acids were normalized to the recovery of the neutral surrogate recovery internal standard. This procedure will accurately quantify basic amino acids in a sample with negligible mineral cation exchange capacity (CEC), such as CPOM and UDOM with low mineral content, and produces little bias in samples dominated by low CEC minerals such as kaolinite (as in Aufdenkampe et al., 2001). However, basic amino acid recoveries can be as low as 10-30% in a matrix of high CEC minerals such as montmorillonite (Cowie and Hedges, 1992). Therefore, presented B/(B + A) values for FPOM and mineral-associated CPOM and UDOM in our data and for FPOM in Hedges et al. (2000) are likely to be lower than actual values, whereas values published by Hedges et al. (1994) are likely to more closely reflect true ambient concentrations because of their use of a basic surrogate recovery internal standard. Last, these differences in the quantitation of basic amino acids are not likely to substantially affect other amino acid parameters, such as $\%T_{AA}C$, $\%T_{AA}N$ (Fig. 9) or even the amino acid degradation index of Dauwe et al. (1999), which only gives moderate weighting to arginine and no weighting to lysine.

Although methodological differences must be considered when comparing B/(B + A) values from different studies, differences in mineralogy may also explain why B/(B + A) values are lower in the Andes and sub-Andes than in the Amazon lowlands. For instance, high inorganic carbon contents in all the fractions (Table 4), especially in the lower reaches, point to a strong influence on mineral surface characteristics by carbonates, which have a net positive surface charge. Such mineralogy has been shown to selectively enrich acidic amino acids onto surfaces (Carter, 1978; Carter and Mitterer, 1978; McKnight et al., 1992), which would draw down values of B/(B + A). The very low B/(B + A) values for UDOM fractions, which have the highest IC/OC ratios in this study (Table 4), may thus offer evidence that the substantial inorganic colloid contents of this fraction might have a role in determining the composition of "dissolved" OM.

The distributions of individual lignin-derived phenols offer a tool for distinguishing between potential plant sources. Ratios of cinnamyl to vanillyl phenols in particular offer the potential to distinguish between dicots and monocots. This is particularly helpful in colder climates, such as the puna, where grass species typically use the C3 photosynthetic pathway and cannot be distinguished from dicots using stable carbon isotope measurements. As might be expected, CPOM and FPOM samples from high elevation sites showed elevated values of C/V, exceeding the range typical of dicots. UDOM samples were uniformly depleted in cinnamyl phenols, although dissolved samples from sites U4 and U7 had the highest C/V values as they did for the coarse and fine fractions. The trend of decreasing C/V from CPOM to FPOM to UDOM for any given sample may be evidence that C/V is sensitive to diagenetic alterations or selective partitioning. Preferential degradation of cinnamyl vs. vanillyl phenols has been previously observed (Hedges and Weliky, 1989; Benner et al., 1991; Opsahl and Benner, 1995), however, no published study has yet tested how selective partitioning might alter lignin phenol signatures.

5. Conclusions

Elemental, isotopic and biochemical compositions of riverine organic matter clearly evolved from Andean source waters to large lowland rivers on their way to joining the Amazon. Similar to previous results from the lower Amazon and from Bolivian tributaries, physical size was the most important

factor in determining the composition and function of riverine organic matter. However, physical size is only a proxy for mineral association, which is the controlling process. This study shows that size is not always a perfect proxy, and that compositional distinctions can sometimes blur between size fractions. For instance, robust sand-sized organo-mineral aggregates in Andean reaches appeared to function as mineral-associated OM similar to that typically found in the fine silt-clay fraction, despite the larger size of these coarse aggregates. Also dissolved organic matter in the high Andes, with its high inorganic colloid content, in some ways behaves as a very fine particulate fraction. Associations between organic and inorganic constituents of this "dissolved" fraction may play an important role in the dynamics of DOM. However, these observations were all discerned from strong compositional signatures of sorptive processes. This study thus provides strong evidence that sorptive processes observed in our previous experimental studies (Aufdenkampe et al., 2001) are broadly applicable and quantitatively important in natural systems.

Acknowledgements

John Hedges unexpected passed away in July 2002, shortly after commenting on the first draft of this manuscript. The legacy that he left cannot be measured only by the quantity and insightfulness of his science, but more importantly by the quality of the friendships he made along the way. A.K.A. is eternally grateful to have been his student, his colleague and his friend. We thank Bonnie Dickson and Jaime Semizo for their dedication, energy and good spirits in the field. We thank David Wilbur, Elizabeth Tsamakis, Michael Peterson and Sonya Remington for their assistance with laboratory analyses. Michael McClain assisted with early stages of field planning, and Rick Keil provided thoughtful comments on the manuscript. This is CAMREX publication 128. This research was funded by US NSF Grants DEB-9408676, INT-9600628 and DEB-9815912 and by NASA LBA Grant NCC5-345.

References

Aalto, R., Maurice-Bourgoin, L., Dunne, T., Montgomery, D.R., Nittrouer, C.A., Guyot, J.-L., 2003. Episodic sediment accumulation on Amazonian flood plains influenced by El Niño/Southern Oscillation. Nature 425, 493–497.

Amelung, W., Zech, W., Zhang, X., Follett, R.F., Tiessen, H., Knox, E., Flach, K.-W., 1998. Carbon, nitrogen, and sulfur pools in particle-size fractions as influenced by climate. Soil Science Society of America Journal 62, 172–181.

Amon, R.M.W., Benner, R., 1996. Bacterial utilization of different size classes of dissolved organic matter. Limnology and Oceanography 41 (1), 41–51.

Aufdenkampe, A.K., Hedges, J.I., Richey, J.E., Krusche, A.V., Llerena, C.A., 2001. Sorptive fractionation of dissolved organic nitrogen and amino acids onto fine sediments within the Amazon Basin. Limnology and Oceanography 46 (8), 1921–1935.

Baldock, J.A., Skjemstad, J.O., 2000. Role of the soil matrix and minerals in protecting natural organic materials against biological attack. Organic Geochemistry 31, 697–710.

Benner, R., 1991. Ultra-filtration for the concentration of bacteria, viruses, and dissolved organic matter. In: Marine Particles: Analysis and Characterization, Geophysical Monograph, vol. 63. American Geophysical Union, pp. 181–185.

Benner, R., Fogel, M.L., Sprague, E.K., 1991. Diagenesis of belowground biomass of *Spartina alterniflora* in salt-marsh sediments. Limnology and Oceanography 36 (7), 1358–1374.

Benner, R., Opsahl, S., Chin-Leo, G., Richey, J.E., Forsberg, B.R., 1995. Bacterial carbon metabolism in the Amazon River system. Limnology and Oceanography 40 (7), 1262–1270.

Bird, M.I., Haberle, S.G., Chivas, A.R., 1994. Effect of altitude on the carbon-isotope composition of forest and grassland soils from Papua New Guinea. Global Biogeochemical Cycles 8 (1), 13–22.

Cai, D.L., Tan, F.C., Edmond, J.M., 1988. Sources and transport of particulate organic carbon in the Amazon River and estuary. Estuarine, Coastal and Shelf Science 26, 1–14.

Carter, P.W., 1978. Adsorption of amino acid-containing organic matter by calcite and quartz. Geochimica et Cosmochimica Acta 42, 1239–1242.

Carter, P.W., Mitterer, R.M., 1978. Amino acid composition of organic matter associated with carbonate and non-carbonate sediments. Geochimica et Cosmochimica Acta 42, 1231–1238.

Cowie, G.L., Hedges, J.I., 1992. Improved amino acid quantification in environmental samples: charge-matched recovery standards and reduced analysis time. Marine Chemistry 37, 223–238.

Cowie, G.L., Hedges, J.I., 1994. Biochemical indicators of diagenetic alteration in natural organic matter mixtures. Nature 369, 304–307.

Cowie, G.L., Hedges, J.I., Prahl, F.G., de Lange, G.J., 1995. Elemental and major biochemical changes across an oxidation front in a relict turbidite: an oxygen effect. Geochimica et Cosmochimica Acta 59, 33–46.

Dauwe, B., Middelburg, J.J., Herman, P.M.J., Heip, C.H.R., 1999. Linking diagenetic alteration of amino acids and bulk organic matter reactivity. Limnology and Oceanography 44 (7), 1809–1814.

Devol, A.H., Hedges, J.I., 2001. Organic matter and nutrients in the mainstem Amazon River. In: McClain, M.E., Victoria, R.L., Richey, J.E. (Eds.), The Biogeochemistry of the Amazon Basin. Oxford University Press, Oxford, pp. 275–306.

Devol, A.H., Forsberg, B.R., Richey, J.E., Pimentel, T.P., 1995. Seasonal variation in chemical distributions in the Amazon

(Solimões) River: a multiyear time series. Global Biogeochemical Cycles 9 (3), 307–328.

Dunne, T., Mertes, L.A.K., Meade, R.H., Richey, J.E., Forsberg, B.R., 1998. Exchanges of sediment between the flood plain and channel of the Amazon River in Brazil. Geological Society of America Bulletin 110 (4), 450–467.

Ertel, J.R., Hedges, J.I., Devol, A.H., Richey, J.E., Ribeiro, M.N.G., 1986. Dissolved humic substances of the Amazon River system. Limnology and Oceanography 31 (4), 739–754.

Gesch, D.B., Verdin, K.L., Greenlee, S.K., 1999. New land surface digital elevation model covers the Earth. EOS 80 (6), 70–71.

Gibbs, R.J., 1967. The geochemistry of the Amazon River System: Part I. The factors that control the salinity and the composition and concentration of the suspended solids. Geological Society of America Bulletin 78, 1203–1232.

Hedges, J.I., Ertel, J.R., 1982. Characterization of lignin by gas capillary chromatography of cupric oxide oxidation products. Analytical Chemistry 54, 174–178.

Hedges, J.I., Stern, J.H., 1984. Carbon and nitrogen determinations of carbonate containing solids. Limnology and Oceanography 29, 657–663.

Hedges, J.I., Weliky, K., 1989. Diagenesis of conifer needles in a coastal marine environment. Geochimica et Cosmochimica Acta 53, 2659–2673.

Hedges, J.I., Clark, W.A., Quay, P.D., Richey, J.E., Devol, A.H., Santos, U.d.M., 1986a. Compositions and fluxes of particulate organic material in the Amazon River. Limnology and Oceanography 31 (4), 717–738.

Hedges, J.I., Ertel, J.R., Quay, P.D., Grootes, P.M., Richey, J.E., Devol, A.H., Farwell, G.W., Schmidt, F.W., Salati, E., 1986b. Organic carbon-14 in the Amazon River system. Science 231, 1129–1131.

Hedges, J.I., Cowie, G.L., Richey, J.E., Quay, P.D., Benner, R., Strom, M., Forsberg, B.R., 1994. Origins and processing of organic matter in the Amazon River as indicated by carbohydrates and amino acids. Limnology and Oceanography 39 (4), 743–761.

Hedges, J.I., Mayorga, E., Tsamakis, E., McClain, M.E., Aufdenkampe, A.K., Quay, P.D., Richey, J.E., Benner, R., Opsahl, S., et al., 2000. Organic matter in Bolivian tributaries of the Amazon River: a comparison to the lower mainstem. Limnology and Oceanography 45 (7), 1449–1466.

Keil, R.G., Montluçon, D.B., Prahl, F.G., Hedges, J.I., 1994. Sorptive preservation of labile organic matter in marine sediments. Nature 370, 549–552.

Keil, R.G., Mayer, L.M., Quay, P.D., Richey, J.E., Hedges, J.I., 1997. Losses of organic matter from riverine particles in deltas. Geochimica et Cosmochimica Acta 61, 1507–1511.

Korner, C., Arnone, J.A.I., 1992. Responses to elevated carbon dioxide in artificial tropical ecosystems. Science 257, 1672–1675.

Ludwig, W., Probst, J.L., Kempe, S., 1996. Predicting the oceanic input of organic carbon by continental erosion. Global Biogeochemical Cycles 10 (1), 23–41.

Mayer, L.M., 1994a. Relationships between mineral surfaces and organic carbon concentrations in soils and sediments. Chemical Geology 114, 347–363.

Mayer, L.M., 1994b. Surface area control of organic carbon accumulation in continental shelf sediments. Geochimica et Cosmochimica Acta 58 (4), 1271–1284.

Mayer, L.M., Keil, R.G., Macko, S.A., Joye, S.B., Ruttenberg, K.C., Aller, R.C., 1998. Importance of suspended particulates in riverine delivery of bioavailable nitrogen to coastal zones. Global Biogeochemical Cycles 12 (4), 573–579.

Mayorga, E., Aufdenkampe, A.K., 2002. Processing of bioactive elements in the Amazon River system. In: McClain, M.E. (Ed.), The Ecohydrology of South American Rivers and Wetlands. IAHS Press, Wallingford, UK, pp. 1–24, IAHS Spec. Pub. No. 6.

Mayorga, E., Aufdenkampe, A.K., Masiello, C.A., Krusche, A.V., Hedges, J.I., Quay, P.D., Richey, J., Brown, T.A., 2005a. Young organic matter as a source of carbon dioxide outgassing from Amazonian rivers. Nature 436, 538–541.

Mayorga, E., Logsdon, M.G., Ballester, M.V.R., Richey, J.E., 2005b. Estimating cell-to-cell land surface flow paths from digital channel networks, with an application to the Amazon basin. Journal of Hydrology 315, 167–182.

McClain, M.E., Richey, J.E., Victoria, R.L., 1995. Andean contributions to the biogeochemistry of the Amazon River system. Bulletin de l'Institute Francais d'Etudes Andines 24 (3), 425–437.

McKnight, D.M., Bencala, K.E., Zeliweger, G.W., Aiken, G.R., Feder, G.L., Thorn, K.A., 1992. Sorption of dissolved organic carbon by hydrous aluminum and iron oxides occurring at the confluence of Deer Creek with the Snake River, Summit County, Colorado. Environmental Science and Technology 26, 1388–1396.

Ménot, G., Burns, S.J., 2001. Carbon isotopes in ombrogenic peat bog plants as climatic indicators: calibration from an altitudinal transect in Switzerland. Organic Geochemistry 32, 233–245.

Neal, C., 2001. Alkalinity measurements within natural waters: towards a standardised approach. The Science of the Total Environment 265, 99–113.

Nelson, P.N., Baldock, J.A., Soulas, G., 1994. Availability of organic carbon in soluble and particle-sized fractions from a soil profile. Soil Biology and Biochemistry 26, 1549–1555.

Oades, J.M., 1989. An introduction to organic matter in mineral soils. In: Dixon, J.B., Weed, S.B. (Eds.), Minerals in Soil Environments, vol. 1. Soil Science Society of America, Madison, pp. 89–159.

Opsahl, S., Benner, R., 1995. Early diagenesis of vascular plant tissues: lignin and cutin decomposition and biogeochemical implications. Geochimica et Cosmochimica Acta 59 (23), 4889–4904.

Peterson, M.L., Lang, S.Q., Aufdenkampe, A.K., Hedges, J.I., 2003. Dissolved organic carbon measurement using a modified high temperature DOC analyzer. Marine Chemistry 81 (1–2), 89–104.

Puhakka, M., Kalliola, R., Rajasilta, M., Salo, J., 1992. River types, site evolution and successional vegetation patterns in Peruvian Amazonia. Journal of Biogeography 19, 651–665.

Quay, P.D., Wilbur, D.O., Richey, J.E., Hedges, J.I., Devol, A.H., Victoria, R., 1992. Carbon cycling in the Amazon River: implications from the ^{13}C compositions of particles and solutes. Limnology and Oceanography 37 (4), 857–871.

Räsänen, M.E., Neller, R., Salo, J., Junger, H., 1992. Recent and ancient fluvial deposition systems in the Amazonian foreland basin, Peru. Geological Magazine 129 (3), 293–306.

Richey, J.E., Meade, R.H., Salati, E., Devol, A.H., Nordin Jr., C.F., dos Santos, U., 1986. Water discharge and suspended

sediment concentrations in the Amazon River: 1982–1984. Water Resources Research 22, 756–764.

Richey, J.E., Melack, J.M., Aufdenkampe, A.K., Ballester, M.V., Hess, L.L., 2002. Outgassing from Amazonian rivers and wetlands as a large tropical source of atmospheric CO_2. Nature 416, 617–620.

Salo, J., Kalliola, R., Häkkinen, I., Mäkinen, Y., Niemelä, P., Puhakka, M., Coley, P.D., 1986. River dynamics and the diversity of Amazon lowland forest. Nature 322, 254–258.

Schimel, D.S., House, J.I., Hibbard, K.A., Bousquet, P., Ciasis, P., Peylin, P., Braswell, B.H., Apps, M.J., Baker, D., Bondeau, A., Canadell, J., Churkina, G., Cramer, W., Denning, A.S., Field, C.B., Friedlingstein, P., Goodale, C., Heimann, M., Houghton, R.A., Melillo, J.M., Moore III, B., Murdiyarso, D., Noble, I., Pacala, S.W., Prentice, I.C., Raupach, M.R., Rayner, P.J., Scholes, R.J., Steffen, W.L., Wirth, C., 2001. Recent patterns and mechanisms of carbon exchange by terrestrial ecosystems. Nature 414, 169–172.

Townsend-Small, A., McClain, M.E., Brandes, J.A., 2005. Contributions of carbon and nitrogen from the Andes Mountains to the Amazon River: evidence from an elevational gradient of soils, plants, and river material. Limnology and Oceanography 50 (2), 672–685.

Wakeham, S.G., Lee, C., Hedges, J.I., Hernes, P.J., Peterson, M.L., 1997. Molecular indicators of diagenetic status in marine organic matter. Geochimica et Cosmochimica Acta 61, 5363–5369.

Waliser, D.E., Somerville, R.C.J., 1994. Preferred latitudes of the Intertropical Convergence Zone. Journal of the Atmospheric Sciences 51 (12), 1619–1639.

Wissmar, R.C., Richey, J.E., Stallard, R.F., Edmond, J.M., 1981. Plankton metabolism and carbon processes in the Amazon River, its tributaries, and floodplain waters, Peru–Brazil, May–June 1977. Ecology 62, 1622–1633.